

Washington University in St. Louis

Washington University Open Scholarship

All Theses and Dissertations (ETDs)

January 2010

Characterization Of Scannable Leaky Wave Antennas Using An Extended Metamaterial Framework

Garrett Gilchrist

Washington University in St. Louis

Follow this and additional works at: <https://openscholarship.wustl.edu/etd>

Recommended Citation

Gilchrist, Garrett, "Characterization Of Scannable Leaky Wave Antennas Using An Extended Metamaterial Framework" (2010). *All Theses and Dissertations (ETDs)*. 461.

<https://openscholarship.wustl.edu/etd/461>

This Thesis is brought to you for free and open access by Washington University Open Scholarship. It has been accepted for inclusion in All Theses and Dissertations (ETDs) by an authorized administrator of Washington University Open Scholarship. For more information, please contact digital@wumail.wustl.edu.

WASHINGTON UNIVERSITY IN ST. LOUIS

School of Engineering and Applied Science

Department of Computer Science and Engineering

Thesis Examination Committee:

Barry Spielman, Chair

Jung-Tsung Shen

Lan Yang

CHARACTERIZATION OF SCANNABLE LEAKY WAVE ANTENNAS USING AN
EXTENDED METAMATERIAL FRAMEWORK

by

Garrett Gilchrist

A thesis presented to the School of Engineering
of Washington University in partial fulfillment of the
requirements for the degree of

MASTER OF SCIENCE

December 2010

Saint Louis, Missouri

Abstract

CHARACTERIZATION OF SCANNABLE LEAKY WAVE ANTENNAS USING AN EXTENDED METAMATERIAL FRAMEWORK

by

Garrett Gilchrist

Master of Science in Electrical Engineering

Washington University in St. Louis, 2010

Research Advisor: Professor Barry Spielman

In the past decade, metamaterials have shown new and exciting ways to treat electromagnetic problems, which have gained popularity within the antenna and microwave circuit fields. A composite right left handed (CRLH) transmission line approach for characterizing the TE_{10} dominate mode rectangular waveguide scannable leaky wave antenna will be treated. This is explained by transmission line theory using the lumped element inductor/capacitor (LC) model. The treatment will develop the ideal lossless CRLH transmission line and show how it can be successfully applied to treat the scannable leaky wave antenna (LWA).

Acknowledgments

I would like to express my highest gratitude to the following people for their continuing support and guidance through this adventure, and without whom this research would have had a decidedly different outcome: my wife and son, Heather and Everett, for their steadfast patience, my mentor, Michael Hurst, PhD., for his enthusiastic guidance through many obstacles, and Professor Barry Spielman, PhD., for asking the hard questions as I navigated an under-explored aspect of metamaterials. I would also like to thank: James Bornholdt, D.Sc., Cyrus Davis, Curt Larson, Terry Ganley, Erik Funk, James Elking, and Kenneth Kraus, D.Sc.

Table of Contents

Abstract.....	ii
Acknowledgments.....	iii
1.0 Introduction.....	1
2.0 Waveguide Impedance/Admittance Derivation.....	3
2.1 TE Mode Equivalent Circuit Model	8
3.0 Antennas	9
3.1 Slot Self Impedance	9
3.2 Slot Equivalent Circuit Model	11
3.3 Mutual Impedance	12
4.0 Metamaterials.....	15
4.1 LC Parameter Extraction.....	16
5.0 Antenna Model.....	24
6.0 Physical Antenna	29
6.1 Test Setup.....	31
6.2 Full Wave Simulation and Measured Results.....	34
6.3 Backlobes.....	35
6.3.1 8.3 GHz Data	36
6.3.2 9.3 GHz Data	37
6.3.3 10.3 GHz Data	39
6.3.4 11.3 GHz Data	40
6.3.5 12.3 GHz Data	42

6.3.6 LC Parameter Extraction Prediction Results	43
7.0 Conclusion	44
8.0 Future Work.....	45
Bibliography	46
Vita.....	52

List of Figures

Figure 1: Longitudinal Slotted Rectangular Waveguide, Top View	3
Figure 2: 2-D Longitudinal Slotted Planar Array, Top View	3
Figure 3: Tilted Slot Rectangular Waveguide, Top View	3
Figure 4: Waveguide Coordinate System	4
Figure 5: Physical Waveguide to Block Diagram.....	8
Figure 6: Waveguide Per Unit Length Circuit Model	9
Figure 7: Physical Slot to Block Diagram	11
Figure 8: Slot Per Unit Length Circuit Model	12
Figure 9: Three Slot Linear Array	12
Figure 10: Coplanar Skewed Dipoles	14
Figure 11: Mutual Impedance between Coplanar Skewed Dipoles.....	15
Figure 12: Ideal Metamaterial Transmission Line Model	16
Figure 13: Half Wavelength Waveguide Section CAD Model	17
Figure 14: Half Wavelength Dipole CAD Model.....	18
Figure 15: Waveguide Cell Circuit Equivalent Model	19
Figure 16: Slot Cell Circuit Equivalent Model.....	19
Figure 17: T-Network	20
Figure 18: Block Diagram of a Two-Port Network	20
Figure 19: T-Network Model.....	22
Figure 20: Angled View of the 10 Slot LWA.....	25
Figure 21: Cross Section of the LWA Looking Down the Waveguide	26

Figure 22: Top Down View of the LWA.....	26
Figure 23: Angled View of the Faceted 3-D Model	27
Figure 24: Close Up View of a Faceted Slot	27
Figure 25: Angled Waveguide View	28
Figure 26: Excited Waveguide Cross Section	29
Figure 27: X-Band Leaky Wave Antenna	29
Figure 28: Leaky Wave Antenna with Excitation and Matched Load.....	30
Figure 29: Leaky Wave Antenna Mounted on the Positioner Pole	31
Figure 30: Test Setup Block Diagram	32
Figure 31: Test Setup, Controller and Network Analyzer Hardware	33
Figure 32: Transmitter View of the Anechoic Chamber	33
Figure 33: Receiver View of the Anechoic Chamber.....	34
Figure 34: Predicted/Measured Coordinate System	35
Figure 35: E- and H-plane Diffraction by a Rectangular Waveguide. <i>Figure Copied From [30 pg. 808]</i>)	36
Figure 36 (8.3 GHz) Predicted Data	36
Figure 37 (8.3 GHz) Measured Data.....	36
Figure 38: (8.3 GHz) Combined Normalized Gain Plot, With a Constant Azimuth (270°) and Varying Elevation	37
Figure 39 (9.3 GHz) Predicted Data	38
Figure 40 (9.3 GHz) Measured Data.....	38
Figure 41: (9.3 GHz) Combined Normalized Gain Plot, With a Constant Azimuth (270°) and Varying Elevation	38

Figure 42 (10.3 GHz) Predicted Data	39
Figure 43 (10.3 GHz) Measured Data.....	39
Figure 44: (10.3 GHz) Combined Normalized Gain Plot, With a Constant Azimuth (270°) and Varying Elevation	40
Figure 45 (11.3 GHz) Predicted Data	41
Figure 46 (11.3 GHz) Measured Data.....	41
Figure 47: (11.3 GHz) Combined Normalized Gain Plot, With a Constant Azimuth (270°) and Varying Elevation	41
Figure 48 (12.3 GHz) Predicted Data	42
Figure 49 (12.3 GHz) Measured Data.....	42
Figure 50: (12.3 GHz) Combined Normalized Gain Plot, With a Constant Azimuth (270°) and Varying Elevation	43
Figure 51: LC Parameter Predictions on a Polar Plot.....	44

1.0 Introduction

The first work performed with the slotted waveguide dates back to 1943 when W. H. Watson introduced the slotted waveguide array [1]. Since then various people have worked with the slotted waveguide. In 1957 Arthur A. Oliner characterized the impedance properties of the narrow radiating slot [2, 3]. In 1963 John F. Ramsay and Boris V. Popovich studied the series inclined slot [4]. Several groups did mutual coupling work throughout the 1960's and 1970's and in the 1981 Robert S. Elliot published an antenna book talking extensively about longitudinal slotted waveguide antennas [5].

The first work theorizing metamaterials started in 1967 – 1968 when Victor Veselago speculated “What if a material exhibited negative permittivity and permeability?” [6]. Nothing came about this thought until 1998 when John Pendry at Imperial College London found a way to create the effects of negative permittivity and permeability [7]. Then David Smith at University of California, San Diego (UCSD) in 2000 combine these effects to create a metamaterial that exhibits both negative permittivity (ϵ) and negative permeability (μ) [8]. In June 2002 three groups introduced a different, more practical approach using transmission line theory: George Eleftheriades, O. Siddiqui and Ashwin Iyer [9], Arthur A. Oliner [10] and Christophe Caloz and Tatsuo Itoh. The last group Christophe Caloz and Tatsuo Itoh wrote a book and many peer reviewed journal papers that spurred this research [11, 12, 13, 14, 15, 16, and 17].

The slotted waveguide has been investigated for many years. It has been implemented in several configurations: off set longitudinal slots, alternating slots on either side of the centerline of the waveguide Figure 1 [5], 2-D planar array Figure 2 [5], and it has also been in a collinear alternating tilted configuration down the centerline of

the waveguide Figure 3 [4]. The latter configuration is the subject of the research described here. With the collinear alternating tilted configuration the slots present a series impedance along the length of the structure and with the series impedance a unique situation arises. The slot, using transmission line theory creates a negative reactance ($-j\chi$) where ($\chi > 0$), which is capacitive. This capacitive value fills a missing piece of the puzzle when modeling the slotted waveguide couched in a metamaterial perspective. The broadside radiation coupled with steering the main beam to the right and left of broadside has caused trouble in the past [18]. Previously, steering the beam through broadside, the main beam would null out or shrink. Also, steering to right and left of broadside had to be done with higher order modes. In this research, the scannable leaky wave antenna (LWA) under investigation is the slotted rectangular waveguide. This antenna allows the main radiation beam to be steered to a desired angle by changing the frequency. A transmission line model, metamaterial-inspired, will be utilized to theoretically predict how the main beam angle varies with frequency. A full wave simulation was performed for the 3-D model then a prototype antenna was measured in an anechoic chamber. Using this combination of approaches it was shown that the scannable leaky wave antenna can radiate at broadside, perpendicular, to the array and that the main radiation beam can be successfully steered to both the left and right of broadside in the dominate mode (TE_{10}). The pervious work by Caloz and Itoh [12] accomplished this for a TEM, less dispersive structure. This work demonstrated that the metamaterial framework is able to successfully treat a highly dispersive scannable structure and overcome broadside radiation limitations.

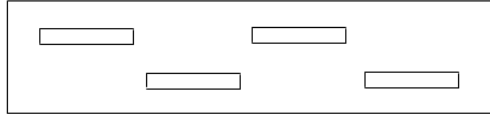


Figure 1: Longitudinal Slotted Rectangular Waveguide, Top View

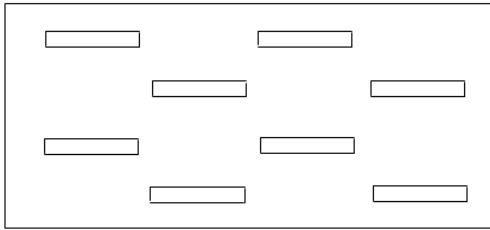


Figure 2: 2-D Longitudinal Slotted Planar Array, Top View

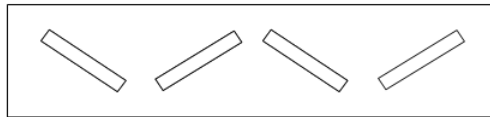


Figure 3: Tilted Slot Rectangular Waveguide, Top View

2.0 Waveguide Impedance/Admittance Derivation

The metamaterial inspired transmission line modeling has four components: two capacitive elements and two inductive elements, this is explained later in the thesis. The waveguide contributes three of the four elements in the transmission line modeling, two inductive and one capacitive; the other capacitive element is from the slot. It is shown below how waveguide portion is derived. From two of Maxwell's Equations, $(\nabla \times E = -j\omega\mu H)$ and $(\nabla \times H = j\omega\epsilon E)$ you can get the following for the loss-free region within the waveguide, (ω) is angular frequency [19, 20].

$$\begin{aligned} \frac{\partial H_z}{\partial y} + \bar{\gamma} H_y &= j\omega\epsilon E_x \quad (\text{a}) \\ \frac{\partial H_z}{\partial x} + \bar{\gamma} H_x &= -j\omega\epsilon E_y \quad (\text{b}) \\ \frac{\partial H_y}{\partial x} - \frac{\partial H_x}{\partial y} &= j\omega\epsilon E_z \quad (\text{c}) \\ \frac{\partial E_z}{\partial y} + \bar{\gamma} E_y &= -j\omega\mu H_x \quad (\text{d}) \\ \frac{\partial E_z}{\partial x} + \bar{\gamma} E_x &= j\omega\mu H_y \quad (\text{e}) \\ \frac{\partial E_y}{\partial x} - \frac{\partial E_x}{\partial y} &= -j\omega\mu H_z \quad (\text{f}) \end{aligned} \quad (1)$$

$$\bar{\gamma} = \bar{\alpha} + j\bar{\beta}$$

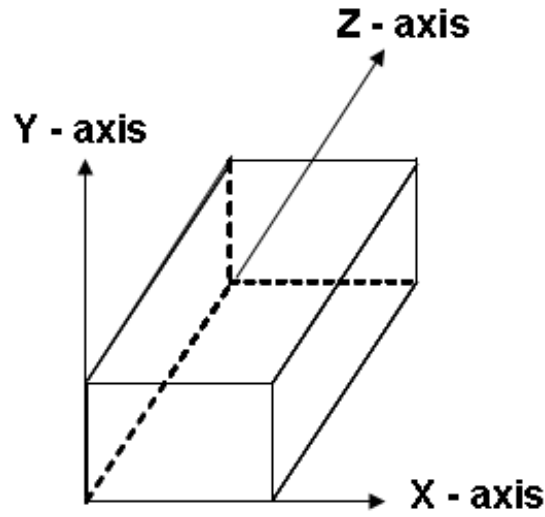


Figure 4: Waveguide Coordinate System

The above equations can be solved for four transverse equations in terms of (E_z) and (H_z) [21].

$$H_x = \frac{j}{k_c^2} \left(\omega \epsilon \frac{\partial E_z}{\partial y} - \beta \frac{\partial H_z}{\partial x} \right) \quad (\text{a})$$

$$H_y = \frac{-j}{k_c^2} \left(\omega \epsilon \frac{\partial E_z}{\partial x} + \beta \frac{\partial H_z}{\partial y} \right) \quad (\text{b})$$

(2)

$$E_x = \frac{-j}{k_c^2} \left(\beta \frac{\partial E_z}{\partial x} + \omega \mu \frac{\partial H_z}{\partial y} \right) \quad (\text{c})$$

$$E_y = \frac{j}{k_c^2} \left(-\beta \frac{\partial E_z}{\partial y} + \omega \mu \frac{\partial H_z}{\partial x} \right) \quad (\text{d})$$

$$k_c^2 = k^2 - \beta^2, \quad k = \frac{2\pi}{\lambda}, \quad \beta = \frac{2\pi}{\lambda_g}, \quad \epsilon = \epsilon_o \epsilon_r, \quad \mu = \mu_o \mu_r, \quad \text{and} \quad \omega = 2\pi f$$

(k_c) is the cutoff wavenumber, (k) is the free space wavenumber, (β) is the propagation constant, (ϵ) is the permittivity with (ϵ_o) being permittivity of free space and (ϵ_r) being the relative permittivity, (μ) is the permeability with (μ_o) being the permeability of free space and (μ_r) being the relative permeability, and (ω) is the angular frequency with (f) being the frequency of interest.

In the longitudinal direction of propagation for the TE-mode ($E_z = 0$) and ($H_z \neq 0$). With this, the above equations reduce to the following.

$$H_x = \frac{-j\beta}{k_c^2} \frac{\partial H_z}{\partial x} \quad (\text{a})$$

$$H_y = \frac{-j\beta}{k_c^2} \frac{\partial H_z}{\partial y} \quad (\text{b}) \quad (3)$$

$$E_x = \frac{-j\omega\mu}{k_c^2} \frac{\partial H_z}{\partial y} \quad (\text{c})$$

$$E_y = \frac{-j\omega\mu}{k_c^2} \frac{\partial H_z}{\partial x} \quad (\text{d})$$

Now dividing the *E-field* by the *H-field* for the characteristic wave impedance of the TE-mode (Z_o^{TE}):

$$Z_o^{\text{TE}} = \frac{E_x}{H_y} = \frac{-E_y}{H_x} = \frac{j\mu\omega}{\gamma} \quad (4)$$

With this said the transmission line analogy for a waveguide can be shown using rectangular coordinate field equations.

$$\frac{\partial H_z}{\partial y} - \frac{\partial H_y}{\partial z} = j\omega\epsilon E_x \quad (a)$$

$$-\frac{\partial H_x}{\partial z} - \frac{\partial H_z}{\partial x} = j\omega\epsilon E_y \quad (b)$$

$$\frac{\partial H_y}{\partial x} - \frac{\partial H_x}{\partial y} = j\omega\epsilon E_z \quad (c) \quad (5)$$

$$\frac{\partial E_z}{\partial y} - \frac{\partial E_y}{\partial z} = -j\omega\mu H_x \quad (d)$$

$$\frac{\partial E_x}{\partial z} - \frac{\partial E_z}{\partial x} = -j\omega\mu H_y \quad (e)$$

$$\frac{\partial E_y}{\partial x} - \frac{\partial E_x}{\partial y} = -j\omega\mu H_z \quad (f)$$

From (5) we are interested in (5a) and (5d). Since ($E_z = 0$) and ($curl_{xy}H = 0$) it is possible to define a magnetic scalar potential (U):

$$H_x = -\frac{\partial U}{\partial x} \quad H_y = -\frac{\partial U}{\partial y}$$

Now using (U), and (5a), (5d), and (2) we will get the following.

$$\frac{\partial}{\partial z} \left(\frac{j\omega\mu}{k_c^2} \frac{\partial H_z}{\partial x} \right) = -j\omega\mu \frac{\partial U}{\partial x} \quad \frac{\partial H_z}{\partial y} - \frac{\partial H_y}{\partial z} = \frac{\omega^2 \mu \epsilon}{k_c^2} \frac{\partial H_z}{\partial y}$$

Therefore

$$\frac{\partial}{\partial z} \left(\frac{j\omega\mu}{k_c^2} H_z \right) = -j\omega\mu U \quad \frac{\partial U}{\partial z} = - \left(\frac{k_c^2}{j\omega\mu} + j\omega\epsilon \right) \left(\frac{j\omega\mu}{k_c^2} H_z \right)$$

The quantity $\left(\frac{j\omega\mu}{k_c^2} H_z \right)$ has voltage dimensions and (U) has current dimensions.

The waveguide series impedance [20]:

$$\frac{\partial V}{\partial z} = -ZI \Rightarrow -Z = \frac{V}{I} \Rightarrow -Z = -j\omega\mu \Rightarrow Z = j\omega\mu \quad (6)$$

The waveguide shunt admittance [20]:

$$\frac{\partial I}{\partial z} = -YV \Rightarrow -Y = \frac{I}{V} \Rightarrow -Y = -\left(\frac{k_c^2}{j\omega\mu} + j\omega\epsilon \right) \Rightarrow Y = \left(\frac{k_c^2}{j\omega\mu} + j\omega\epsilon \right) \quad (7)$$

There is a useful relationship between the constitutive parameters $(\epsilon\mu)$ and per unit length parameters $(C'L')$ [22]:

$$(C'L') = (\epsilon\mu) \quad (8)$$

2.1 TE Mode Equivalent Circuit Model

Below is a TE mode equivalent circuit flow chart of how a section of waveguide is represented with a complex series impedance and shunt admittance per unit length. The sinusoidal wave indicates the direction of propagation in the waveguide. The (Z') , (Y') , (C') , and (L') are per unit length values.

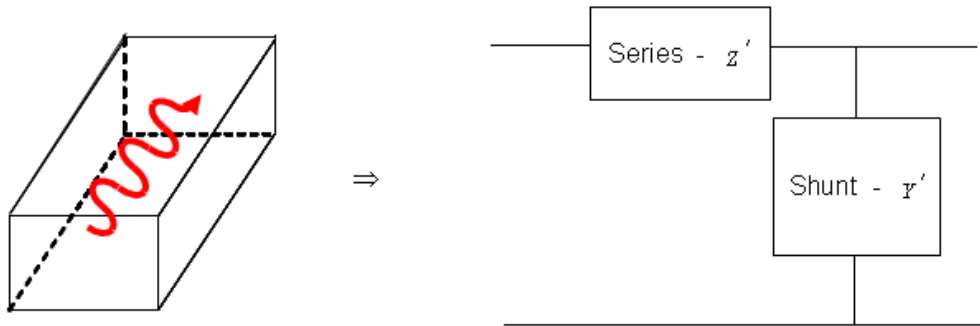


Figure 5: Physical Waveguide to Block Diagram

$$Z' = R' + jX' \Rightarrow Z' = j\omega L' \quad (9)$$

$$Y' = G' + jB' \Rightarrow Y' = j\omega C' + \frac{k_c^2}{j\omega L'} \quad (10)$$

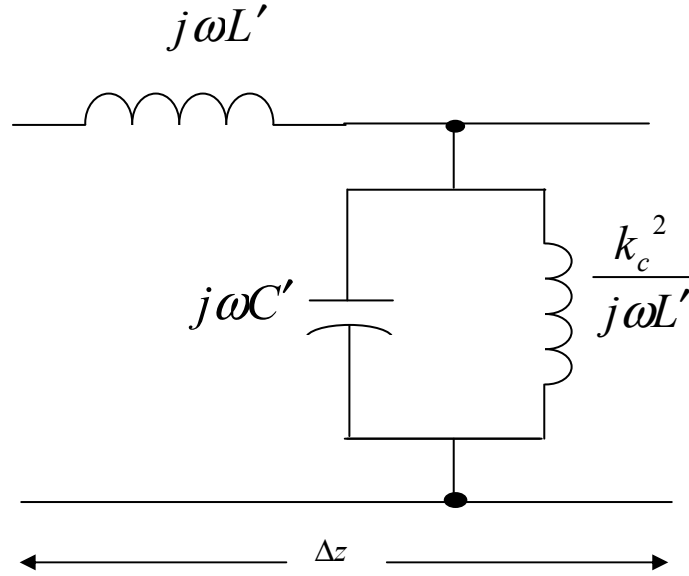


Figure 6: Waveguide Per Unit Length Circuit Model

3.0 Antennas

3.1 Slot Self Impedance

Impedance (Z) is defined as the ratio between phasor voltage (V) and phasor current (I).

$$Z = \frac{V}{I} \quad (11)$$

The same is true for the terminal impedance of a half wave dipole [23].

$$Z_{11} = \frac{V_{11}}{I_1} \quad (12)$$

According to John D. Kraus [23] § 10.3 there is a good derivation using the Sine and Cosine Integrals where the dipole impedance becomes complex with a real and imaginary (inductive) part:

$$Z = R + jX \quad (13)$$

with

$$R = 30Ci_n(2\pi) \quad (14)$$

$$X = 30Si(2\pi) \quad (15)$$

where $Ci(x) = \text{Cosine Integral}$, $n = \text{odd number multiple}$, and $Si(x) = \text{Sine Integral}$. The cosine and sine integrals are defined mathematically as [23]:

$$Ci(x) = \int_{\infty}^x \frac{\cos(v)}{v} dv \quad (16)$$

$$Si(x) = \int_0^x \frac{\sin(v)}{v} dv \quad (17)$$

The above impedance value is for non-resonant antennas. Resonant antennas just have a real (R) part. Then, H.G Booker used Babinet's Principle (optics) in electromagnetics to relate the known impedance of a dipole antenna to calculate the impedance of a complementary slot [24]:

$$Z_d Z_s = \frac{\eta^2}{4} \quad (18)$$

where

$Z_d = \text{Dipole Impedance}$

$Z_s = \text{Slot Impedance}$

$$\eta = \sqrt{\frac{\mu_o}{\epsilon_o}} = \text{Free Space Impedance (376.7 } \Omega)$$

$$Z_s = \frac{\eta^2}{4Z_d} \quad (19)$$

Using the dipole impedance from above:

$$Z_s = \frac{\eta^2}{4} \frac{1}{(R_d + jX_d)} \Rightarrow Z_s = R_s - jX_s \quad (20)$$

Now the impedance is complex with a real and imaginary (capacitive) part.

3.2 Slot Equivalent Circuit Model

Below is a slot equivalent circuit flow chart of how the tilted slot in the waveguide is represented with a complex series impedance per unit length. The (Z') , (R') , and (C') are per unit length values. The (R') in Figure 8 captures the radiation behavior of the slot.



Figure 7: Physical Slot to Block Diagram

$$Z' = R' + jX' \Rightarrow Z' = R' + \frac{1}{j\omega C'} \quad (21)$$

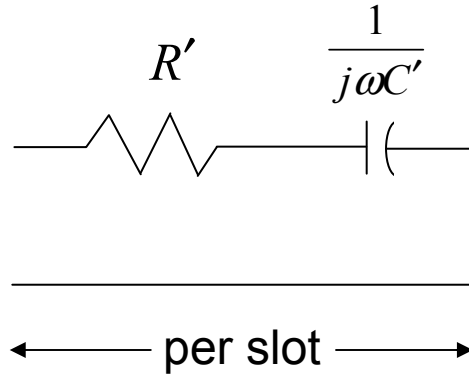


Figure 8: Slot Per Unit Length Circuit Model

3.3 Mutual Impedance

When dealing with more than one radiator, mutual impedance has to be taken into account.

$$Z_{ij} = \frac{V_i}{I_j} \quad (22)$$

This means the total impedance (Z_{Ti}) of one radiator is dependant on the other radiators.

In Figure 9 there is a linear array of three slots and using the ($N \times N$) matrix, (23), for a three port network the total impedance of each slot can be found.

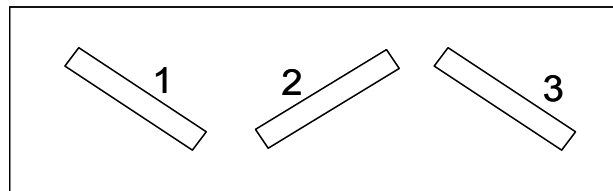


Figure 9: Three Slot Linear Array

$$\begin{bmatrix} V_1 \\ V_2 \\ V_3 \end{bmatrix} = \begin{bmatrix} Z_{11} & Z_{12} & Z_{13} \\ Z_{21} & Z_{22} & Z_{23} \\ Z_{31} & Z_{32} & Z_{33} \end{bmatrix} \begin{bmatrix} I_1 \\ I_2 \\ I_3 \end{bmatrix} \quad (23)$$

Distributing the current using matrix algebra for the first slot in the array, the voltage will be:

$$V_1 = Z_{11}I_1 + Z_{12}I_2 + Z_{13}I_3$$

Now divide both sides by the current of the first slot (I_1) to get the total impedance of the slot.

$$Z_{T1} = \frac{V_1}{I_1} = Z_{11} + Z_{12} \frac{I_2}{I_1} + Z_{13} \frac{I_3}{I_1} \quad (24)$$

Without including the mutual impedance from the other slots will result in, an incorrect total slot impedance. Doing this for the rest of the slots will result in the following equations.

$$V_2 = Z_{21}I_1 + Z_{22}I_2 + Z_{23}I_3 \quad \Rightarrow \quad Z_{T2} = \frac{V_2}{I_2} = Z_{21} \frac{I_1}{I_2} + Z_{22} + Z_{23} \frac{I_3}{I_2}$$

$$V_3 = Z_{31}I_1 + Z_{32}I_2 + Z_{33}I_3 \quad \Rightarrow \quad Z_{T3} = \frac{V_3}{I_3} = Z_{31} \frac{I_1}{I_3} + Z_{32} \frac{I_2}{I_3} + Z_{33}$$

The LWA used in this thesis has ten slots down the center of the waveguide with a tilt. This may be referred to as coplanar skewed slots. In a center line configuration of series slots, the angle ($\pm\theta$), in Figure 10, from horizontal has to be greater than (0 degrees) in order to interrupt the longitudinal current flow in the top broadwall of the waveguide to

cause radiation [4]. Without the tilt in this configuration the antenna will not radiate. In the research done in this thesis, the greater the tilt from horizontal the larger gain you will get with the antenna. Figure 11 shows mutual impedance between two coplanar dipoles separated by (1.0λ) with λ being wavelength. The dipoles are rotated about the center, Figure 10, when $(\psi = 0)$ both slots are vertical and when $(\psi = 180)$ both slots are horizontal. The dashed lines in Figure 10 show the vertex of the angle between the dipoles. Figure 11 shows the reactance is more sensitive to the angle between the dipole and the greatest mutual impedance occurs when there is no angle between the dipoles $(\psi = 0)$. The plot was duplicated from [25, 26].

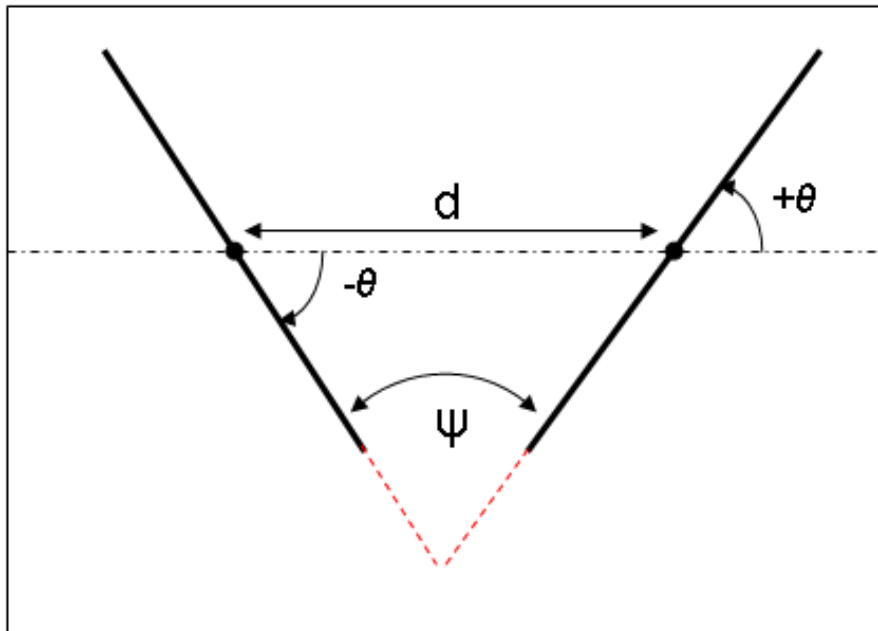


Figure 10: Coplanar Skewed Dipoles

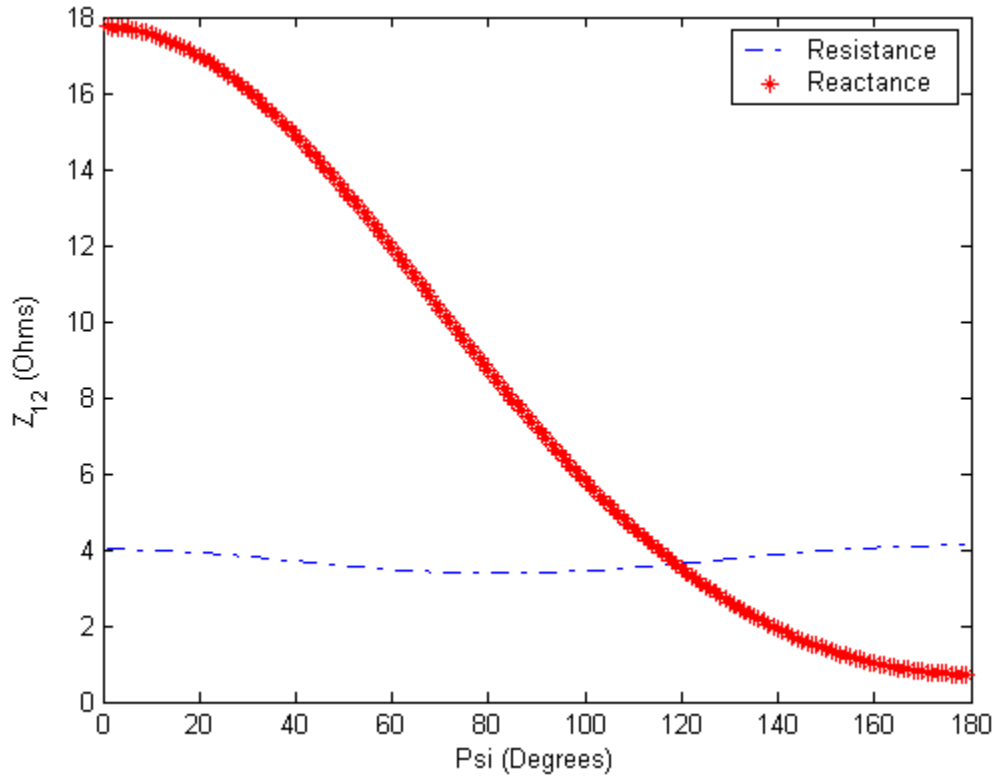


Figure 11: Mutual Impedance between Coplanar Skewed Dipoles

4.0 Metamaterials

Metamaterials is a relatively new area of research in electromagnetics/antennas.

Figure 12 shows an ideal lossless cell from a multi-cell metamaterial transmission line model. This model has series impedance (Z) and shunt admittance (Y) per unit cell.

Using the model inspired by a metamaterial modeling approach applied to the LWA, it can be shown the main beam radiation is accurately predicted.

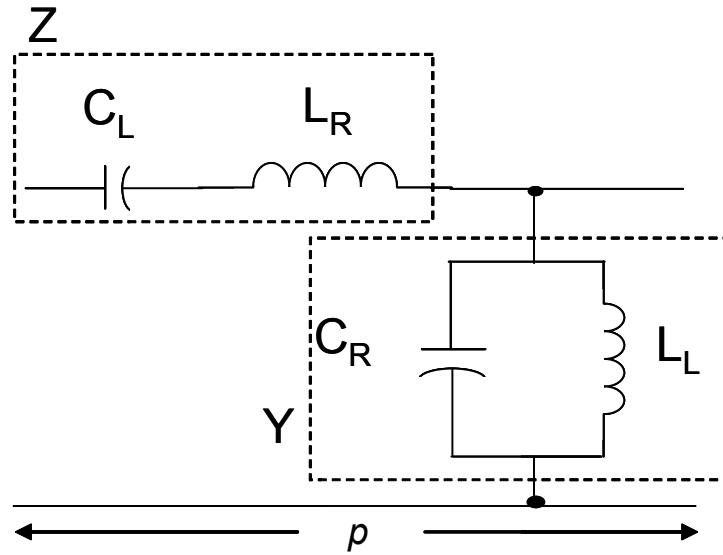


Figure 12: Ideal Metamaterial Transmission Line Model

4.1 LC Parameter Extraction

The LC parameter extraction is an approach to evaluate the series/shunt inductances (L) and capacitances (C) for the transmission line model. This approach allows a design to be predicted without creating the entire structure. The idea is to predict radiation angle of the main beam of the radiating structure by extracting the capacitances and inductances of one cell of the structure. This approach stems from work published by Caloz, Atsushi, and Itoh who used it to extract the right handed capacitance (C_R), right handed inductance (L_R), left handed capacitance (C_L), and left handed inductance (L_L) for a transverse electromagnetic (TEM) structure [11]. The structure they used was a microstrip antenna which is a transverse electromagnetic (TEM) mode, two conductor, ground plane and top structure separated by a dielectric [11]. A similar approach is used in this research to treat a more dispersive transmission structure.

The LC Parameter Extraction approach:

- Have the initial design and run physical components of the cell model in a full wave simulator to evaluate the scattering parameters (S-parameters).
- Convert the S-parameters to impedance parameters (Z-parameters) or admittance parameters (Y-parameters).
- Solve for each of the right/left handed L's and C's.
- Use the right/left handed L's and C's to determine the phase constant (β).
- Place (β) in the main beam angle equation.

The approach was employed in this research to extract the L's and C's for the LWA. The LWA, tilted slot rectangular waveguide, under investigation is a dispersive radiating structure. In order to get the impedance parameters first the design has to be broken into the components of the cell and predicted separately, the waveguide section is predicted separate from the slot and vice versa. Figure 13 is the half wavelength waveguide section that was run in the full wave simulator to get the S-parameters for the waveguide portion of the model. Figure 14 is the half wavelength dipole that was evaluated in the full wave simulator to get the impedance values for the slot portion of the model.

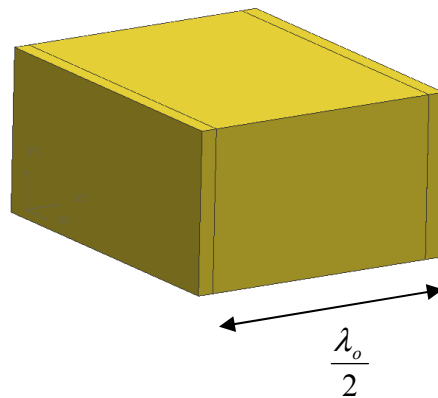


Figure 13: Half Wavelength Waveguide Section CAD Model

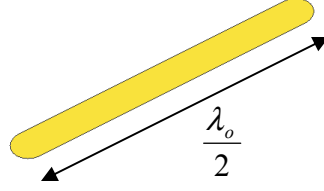


Figure 14: Half Wavelength Dipole CAD Model

The half wavelength waveguide prediction gave the S-parameters:

$$\begin{bmatrix} S_{11} & S_{12} \\ S_{21} & S_{22} \end{bmatrix} \quad (25)$$

The S-parameters are then converted in to Z- parameters using standard conversion equations [21]:

$$Z_{11} = Z_0 \frac{(1 + S_{11})(1 - S_{22}) + S_{12}S_{21}}{(1 - S_{11})(1 - S_{22}) - S_{12}S_{21}} \quad (a)$$

$$Z_{12} = Z_0 \frac{2S_{12}}{(1 - S_{11})(1 - S_{22}) - S_{12}S_{21}} \quad (b)$$

$$Z_{21} = Z_0 \frac{2S_{21}}{(1 - S_{11})(1 - S_{22}) - S_{12}S_{21}} \quad (c) \quad (26)$$

$$Z_{22} = Z_0 \frac{(1 - S_{11})(1 + S_{22}) + S_{12}S_{21}}{(1 - S_{11})(1 - S_{22}) - S_{12}S_{21}} \quad (d)$$

(Z_0) is the characteristic impedance of the waveguide. The Z-matrix is symmetric and due to reciprocity ($Z_{12} = Z_{21}$). Solving for the waveguide portion:

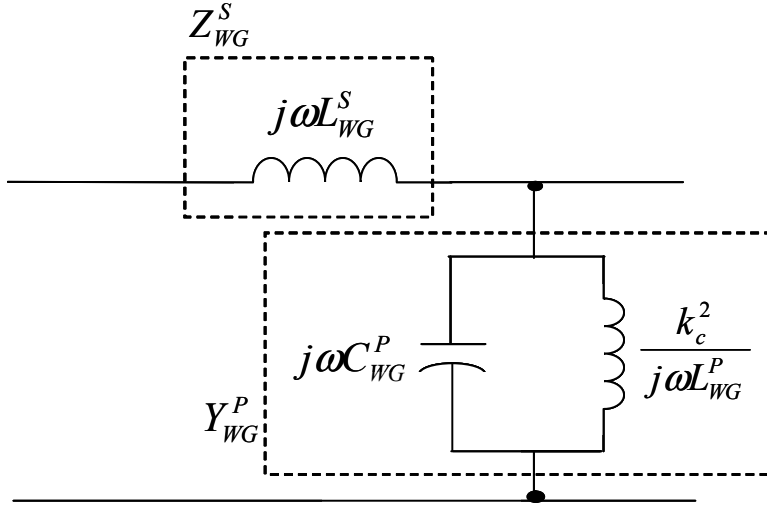


Figure 15: Waveguide Cell Circuit Equivalent Model

$$Z_{WG}^S = j\omega L_{WG}^S \quad (27)$$

$$Y_{WG}^P = j\omega C_{WG}^P + \frac{k_c^2}{j\omega L_{WG}^P} \quad (28)$$

The half wavelength dipole's prediction gave the impedance value which is converted to a slot impedance value by using the Babinet-Booker Principle mentioned above. The slot impedance has a real component in it however; the real part can be neglected for the phase calculation (β).

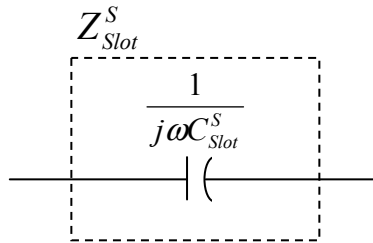


Figure 16: Slot Cell Circuit Equivalent Model

$$Z_{Slot}^S = \frac{1}{j\omega C_{Slot}^S} \quad (29)$$

The Z- parameters for the waveguide are:

$$Z_{WG} = \begin{bmatrix} Z_{11}^{WG} & Z_{12}^{WG} \\ Z_{21}^{WG} & Z_{22}^{WG} \end{bmatrix} = \begin{bmatrix} \frac{1}{Y_{WG}^P} + Z_{WG}^S & -\frac{1}{Y_{WG}^P} \\ -\frac{1}{Y_{WG}^P} & \frac{1}{Y_{WG}^P} + Z_{WG}^S \end{bmatrix} \quad (30)$$

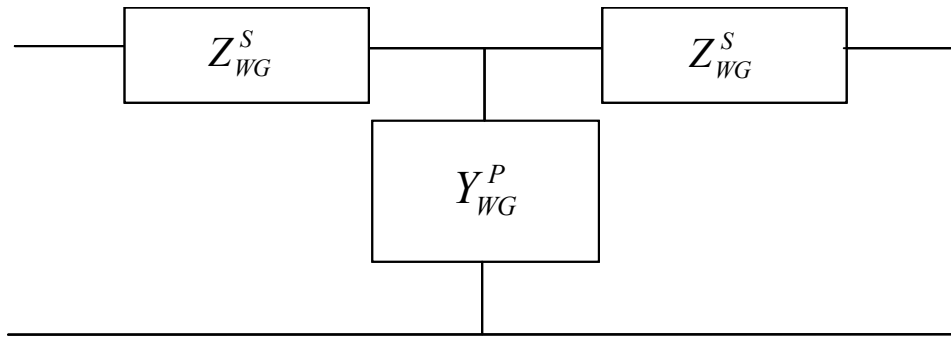


Figure 17: T-Network

The negative sign for (Z_{12}^{WG}) and (Z_{21}^{WG}) in (30) conforms to the convention of having the current coming into either side of two port network as shown in Figure 18 [27].

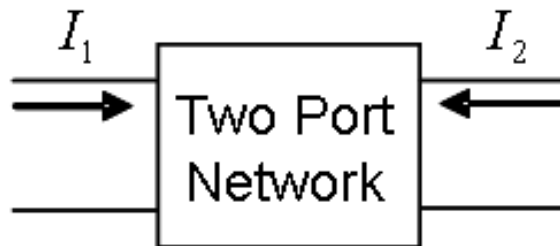


Figure 18: Block Diagram of a Two-Port Network

The Z-parameter for the slot is:

$$Z_{Slot} = Z_{11}^{Slot} = Z_{Slot}^S \quad (31)$$

Each of the inductances and capacitances in (27, 28, and 29) are:

$$L_{WG}^S = \frac{2}{j\omega} (Z_{11} - Z_{12}) \quad (32)$$

$$C_{Slot}^S = \frac{1}{j2\omega Z_{11}} \quad (33)$$

$$C_{WG}^P = \frac{1}{j\omega} \left(Y - \frac{k_c^2}{j\omega L_{WG}^P} \right) \quad (34)$$

$$L_{WG}^P = \frac{1}{j\omega} \left(\frac{k_c^2}{Y - j\omega C_{WG}^P} \right) \quad (35)$$

In order to solve for the parallel capacitance and inductance see Figure 15, the partial derivative of (Y_{WG}^P) is taken with respect to angular frequency (ω):

$$\left(\frac{\partial Y_{WG}^P}{\partial \omega} \right) = 0 \quad (36)$$

This is done to create a second equation in order to solve for each variable. Once the partial derivative is taken, it is set equal to zero and solved, for either the capacitance or inductance. The right/left hand L's and C's for the metamaterials model are shown below.

Series Impedance:

$$C_L = C_{Slot}^S = \frac{1}{j2\omega Z_{11}^{Slot}} \quad (37)$$

$$L_R = L_{WG}^S = \frac{2}{j\omega} (Z_{11}^{WG} - Z_{12}^{WG}) \quad (38)$$

The “2” in the denominator of (37) and the numerator of (38) results from representing these elements as a T-network that combines properly with elements adjacent in the metamaterials transmission line model Figure 19.

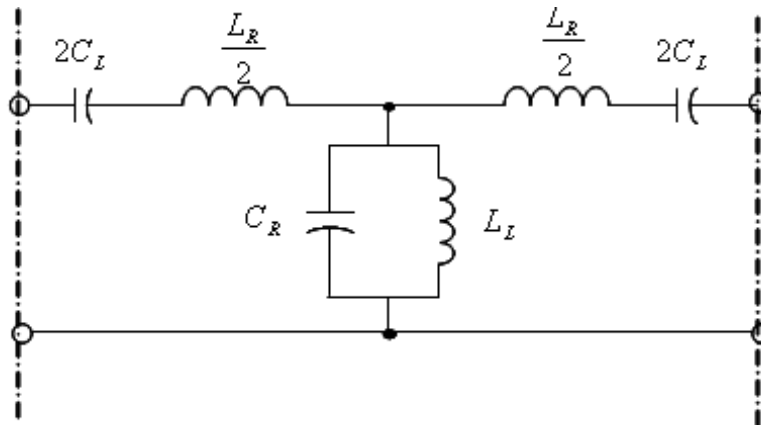


Figure 19: T-Network Model

Shunt Admittance:

$$C_R = C_{WG}^P = \frac{Y_{WG}^P}{j2\omega} \quad (39)$$

$$L_L = L_{WG}^P = \frac{2k_c^2}{j\omega Y_{WG}^P} \quad (40)$$

The LC extracted parameters are: $L_L = 6.683$ nH, $C_L = 0.149$ pF, $L_R = -12.886$ μ H, and $C_R = -0.349$ pF. These four variables L_L , C_L , L_R , and C_R , are used to calculate the phase constant (β) with the following equation [11]:

$$\beta(\omega) = \frac{1}{p} \left(\omega \sqrt{L_R C_R} - \frac{1}{\omega \sqrt{L_L C_L}} \right) \quad (41)$$

(p) is the physical cell size. Once (β) is known for each of the different frequencies, it can be substituted in the following equation to determine the main beam angle (θ_{MB}) for an alternating titled slot LWA [5, 11].

$$\theta_{MB} = \cos^{-1} \left(\frac{\beta}{k} - \frac{\lambda}{2d} \right) \quad (42)$$

(42) is the $psi(\psi)$ variable from array theory, which is used in many variations of the array factor (AF) equation [28, 29].

$$AF = \sum_{n=1}^N e^{j(n-1)\psi} \quad (43)$$

where

$$\psi = k_o d \cos(\theta) - \beta d \quad (44)$$

For the tilted slot rectangular waveguide array case it is [28]:

$$k_o d \cos(\theta) - \beta d + \pi = 2m\pi; \quad (m = 0,1,2,3\dots) \quad (45)$$

Here $\left(k_o = \frac{2\pi}{\lambda_o}\right)$, d is the inter-element slot spacing, β is given by (41), and θ is solved for, $(\theta = \theta_{MB})$ for (42) and (45). The addition of (π) accounts for the possible (180°) phase change due to the tilt of the slot [4, 28]. The calculation from (42) is only accurate if there is negligible mutual coupling between the slots in the array [4, 29]. Using the dispersive tilted slot rectangular waveguide this is not the case as the LC parameter extraction predicted results will show.

5.0 Antenna Model

The full wave simulator used to predict the main beam angle (θ_{MB}) for the LWA is (*In-situ Large ANtenna Aperture & Array Simulations*) (*Code for the Analysis of Radiators on LOssy Surfaces*) (ILANS CARLOS). CARLOS implements the method of moments (MoM) analysis technique. This analysis will give the solution for a fully arbitrary three dimensional (3-D) complex radiator. The solutions are obtained for perfectly conducting bodies (PEC) as well as partially penetrable ones. The electromagnetic solution is based

on the electric field integral equation (EFIE). CARLOS uses planar triangular patch representation for all of the surfaces and boundaries of the radiator [30].

CARLOS was applied to the 3-D computer aided design (CAD) model of the desired structure. Figure 20 – Figure 22 show different views of the 3-D model used in the full wave simulation. Figure 20 shows a 3-D view of the leaky wave antenna model. Figure 21 shows the 3-D view with the ends removed to reveal the waveguide wall thickness which is (0.254 cm) thick. Figure 22 looking top down on the model shows the (10 slots) in the antenna, there is $(0.51\lambda_g)$ center element spacing, the slot length is $(0.5\lambda_0)$, and the slot width is (0.159 cm).

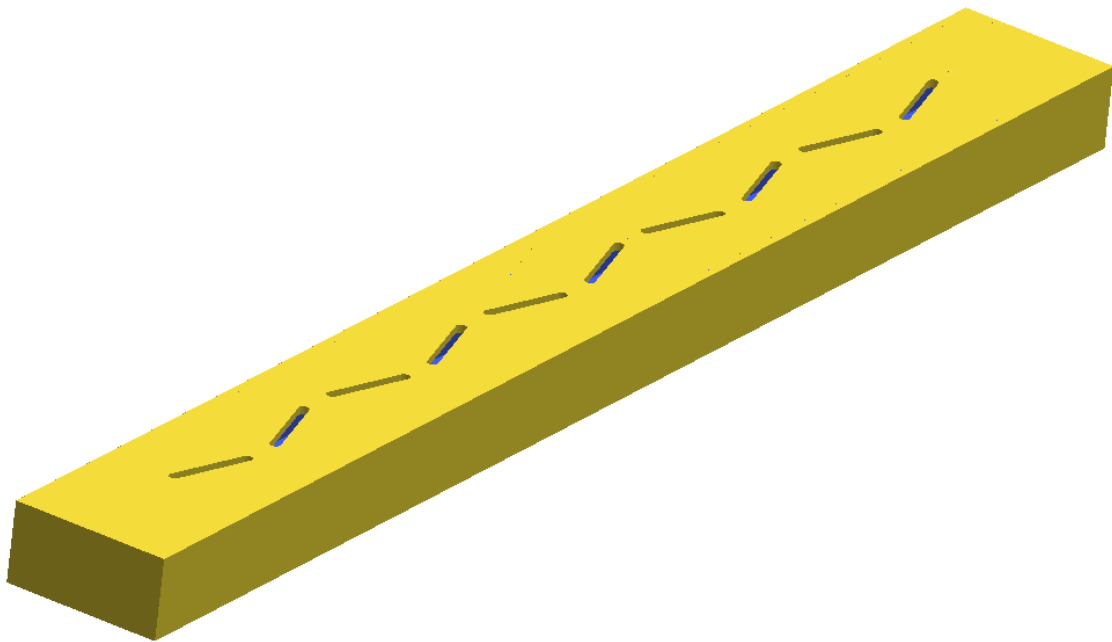


Figure 20: Angled View of the 10 Slot LWA

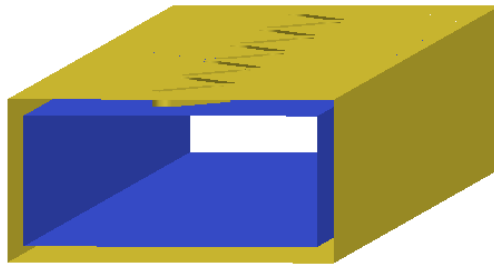


Figure 21: Cross Section of the LWA Looking Down the Waveguide



Figure 22: Top Down View of the LWA

After the structure is designed in the CAD environment it must be sub-divided into surface facets. This means the structure is broken into small triangular segments in order to calculate the currents on the surface. Once the interactions between each of the facets are known the currents are determined and the $(\vec{E} - field)$ and $(\vec{H} - field)$ for the problem can be solved. Figure 23 and Figure 24 shows the faceted model used in the simulation. Notice the grid is finer around each of the slots; this is to capture the detail of the slot. For example there are ten facets at each end of each slot to reveal the rounded slot ends. Figure 23 shows the facetized model with (104661 unknowns) and the grid density is $(\lambda/20)$. Figure 24 shows a close-up view of a slot and the grid density. The blue outline helps identify the slot edges in the grid.

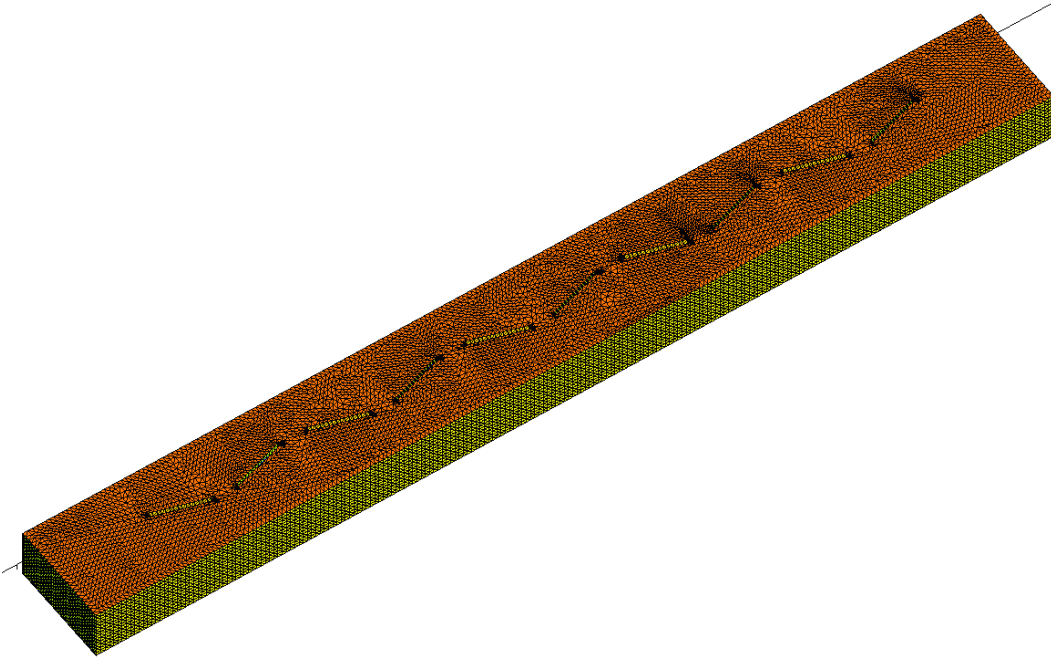


Figure 23: Angled View of the Faceted 3-D Model

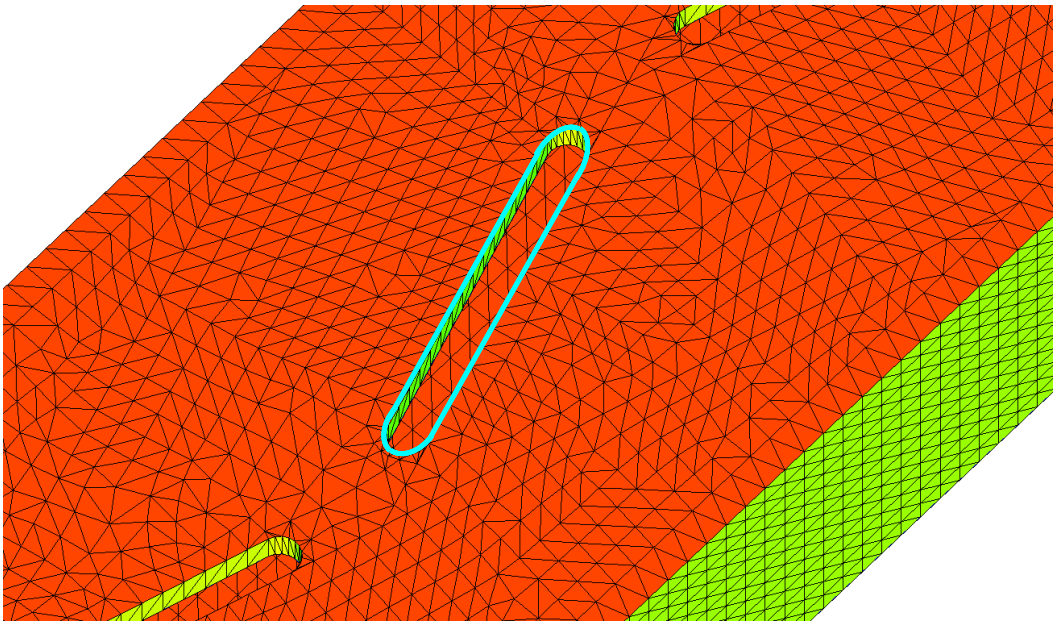


Figure 24: Close Up View of a Faceted Slot

Figure 25 shows the excitation of the LWA. This figure shows the TE_{10} mode in the waveguide and also shows the slots being excited. The subscripts in (TE_{mn}) are the number of half cycles of the propagating mode. The (m) is the number of half cycles in the x-direction and (n) is the number of half cycles in the y-direction. To show the range of excitation the dark blue shows no excitation and the red is peak excitation.

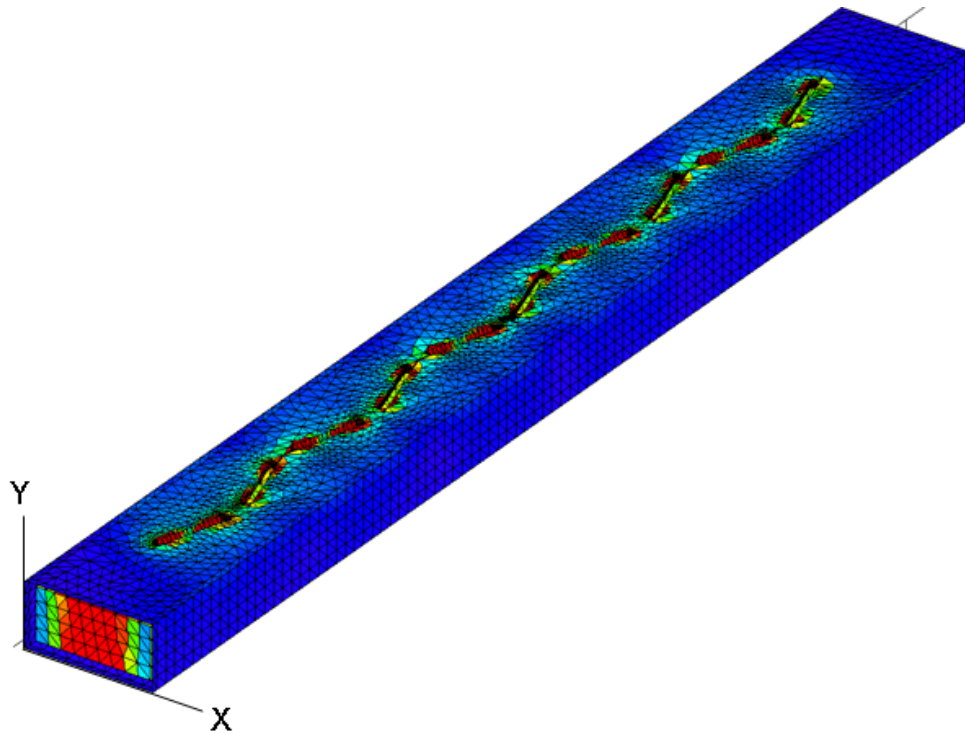


Figure 25: Angled Waveguide View

Figure 26 is a cross section looking down the LWA. Here the color presentation shows TE_{10} mode clearly dies off at the sidewalls and peaks in the middle. This view also shows the closed region of the model, the dark blue perimeter. At the top of the TE_{10} mode are the excited slot walls.

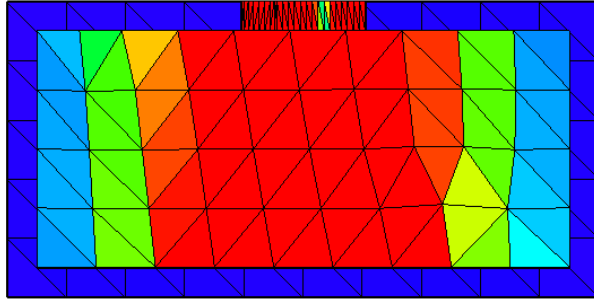


Figure 26: Excited Waveguide Cross Section

6.0 Physical Antenna

The parameters below give the physical dimension of the antenna depicted in Figure 27:

WR-90 X-Band rectangular copper waveguide (0.254 x 0.127) meters

Antenna Length = 0.229 meters

Element Spacing = 0.019 meters

Slot Length = 0.015 meters

Slot Width = 0.002 meters

Number of Slots = 10

Tilt = $\pm 17^\circ$

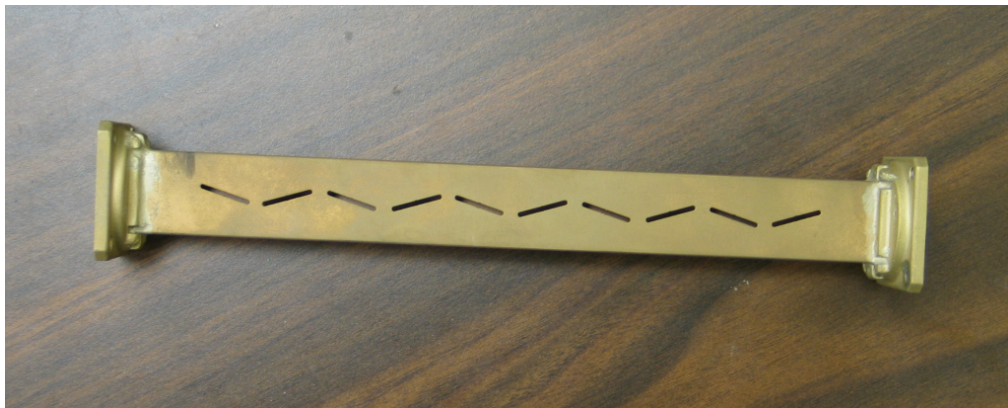


Figure 27: X-Band Leaky Wave Antenna

In Figure 28 the antenna has attachments at both ends. The gray box on the left end of the LWA is the probe feed excitation for the antenna. There is a probe located at the bottom of the small gray box and launches the wave in the guide. The antenna was excited with a TE_{10} mode this is the fundamental mode for the waveguide. The copper section between the excitation and the antenna is a spacer to position the excitation in the anechoic chamber on the pole. At the other end of the antenna is a blue rectangular box which is the load, this is a match load for the X-Band (TE_{10}) mode and does not allow any reflections in the antenna.



Figure 28: Leaky Wave Antenna with Excitation and Matched Load

Figure 29 is the antenna mounted in the anechoic chamber on the positioner pole. The positioner moves in both theta and phi directions. The blueish box with the circular disk allows the phi-direction movement. The box itself is seen in the measurements for the different frequencies, this will be discussed later.

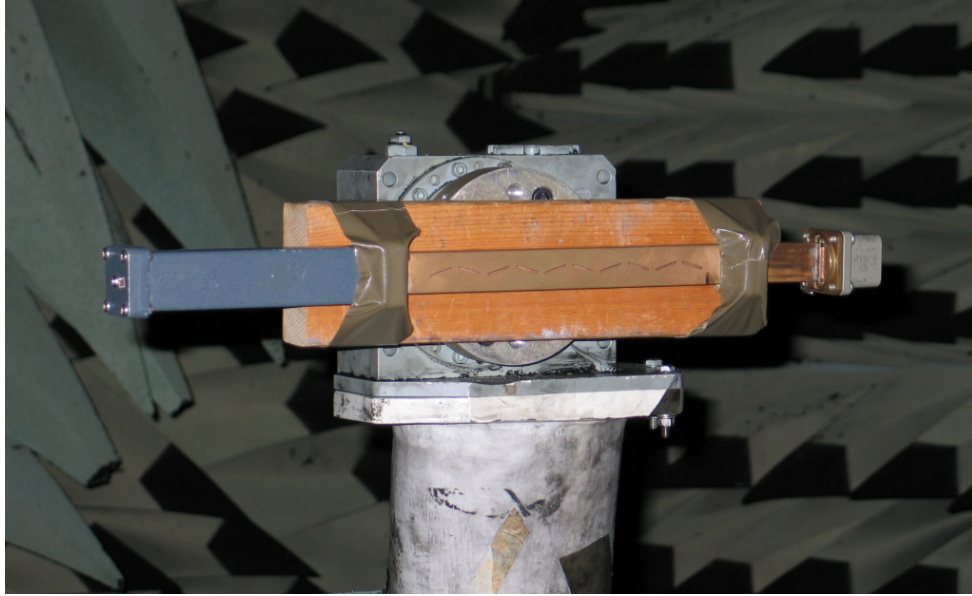


Figure 29: Leaky Wave Antenna Mounted on the Positioner Pole

6.1 Test Setup

The measurements of the antenna were taken in an anechoic chamber. Figure 30 is a block diagram of the test setup. The transmitter (TX) is a Scientific Atlanta Standard Gain Horn Model 12 - 8.20, Frequency Range (8.2 - 12.4 GHz) and the receiver (RX) is the leaky wave antenna. The measurement system controller is a desktop PC which collects the measurement data. The network analyzer is an Agilent Technologies E8363B 10MHz - 40GHz, PNA Series Network Analyzer.

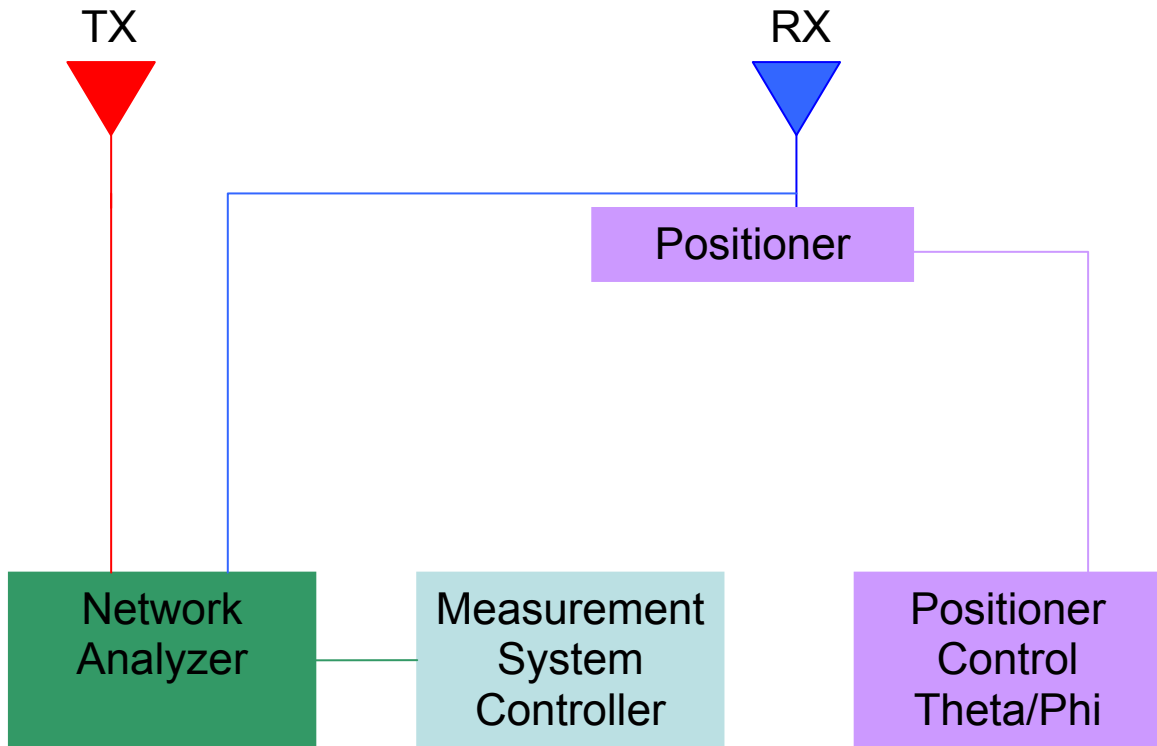


Figure 30: Test Setup Block Diagram

The objects in Figure 31 are the network analyzer on the left, the Measurement System Controller monitor in the middle, and the Positioner Control on the right.

Figure 32 is looking into the anechoic chamber from the transmitting horn antenna position. The positioner in the chamber spins on an imaginary axis from the floor to the ceiling allowing the theta angles in the measurements. The measurements taken in this research hold the phi positioner constant while the theta positioner varies. Figure 33 is looking at the transmitting antenna from the positioner.

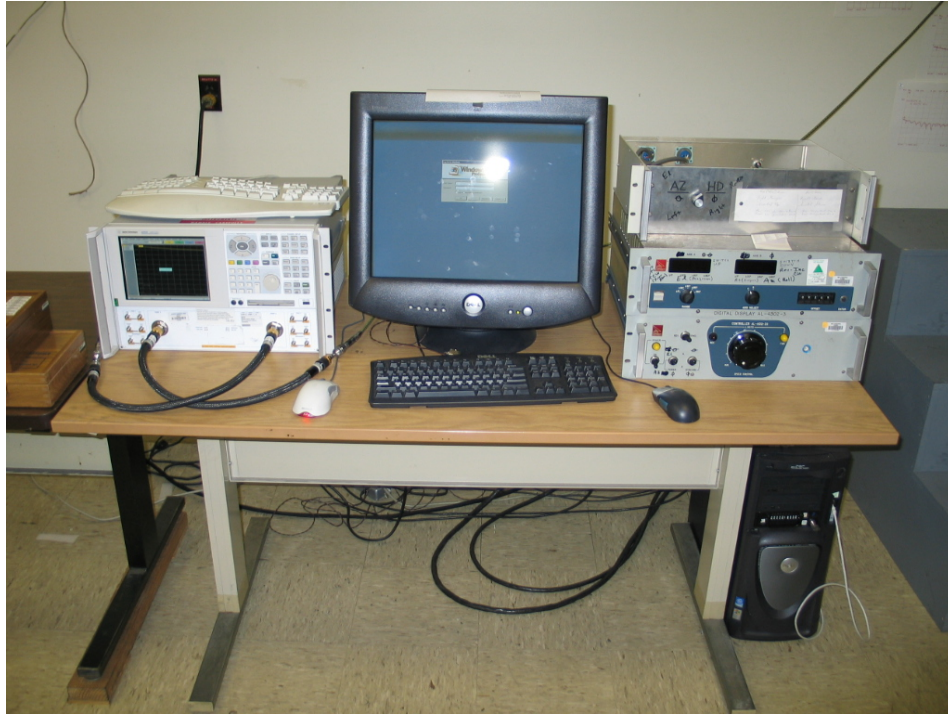


Figure 31: Test Setup, Controller and Network Analyzer Hardware

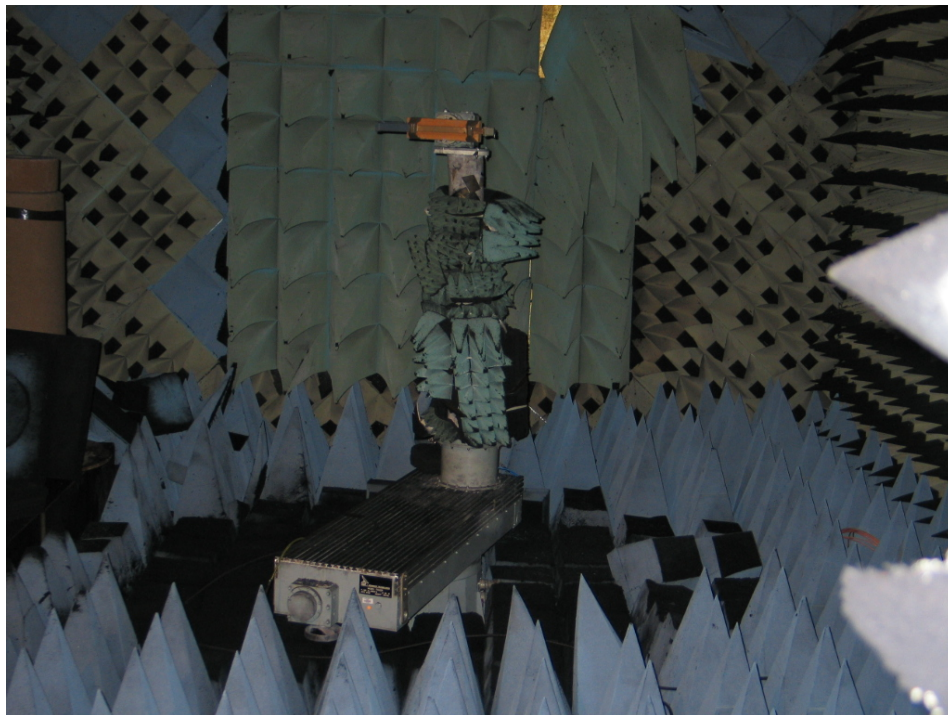


Figure 32: Transmitter View of the Anechoic Chamber



Figure 33: Receiver View of the Anechoic Chamber

6.2 Full Wave Simulation and Measured Results

The following radiation gain patterns are the full wave simulator (predicted) data using CARLOS and the measured data from the test setup mentioned above. The patterns are far field conic cuts with a constant phi of (270 degrees) and a varying theta (0 – 360 degrees). The plots are normalized to peak gain. Figure 34 is the coordinate system used for the data.

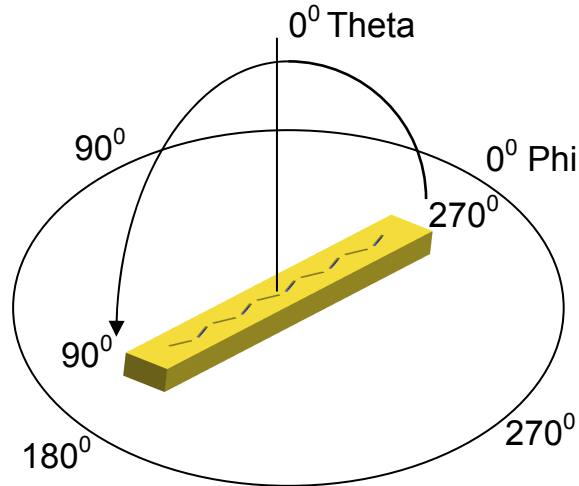


Figure 34: Predicted/Measured Coordinate System

6.3 Backlobes

The leaky wave antenna's predicted and measured data shown below are not predicted or measured with an infinite ground plane. With this said, the finite length of the broadwall, where the slots are, of the antenna (2.54 cm) has some effects that would not be there if it were possible to have an infinite ground plane behind the antenna during data collection.

The effects are backlobes. The currents that are induced on the broadwall during radiation travel along the surface. When those currents reach the edge of the surface they will radiate and diffract around the edge of the surface and radiate in a different direction.

With this diffraction you will get backlobes. The diffraction can be explained by Geometric Theory of Diffraction (GTD) [29, 31]. Figure 35 shows the edge diffraction from a finite surface mounted on the end of a truncated rectangular waveguide [31].

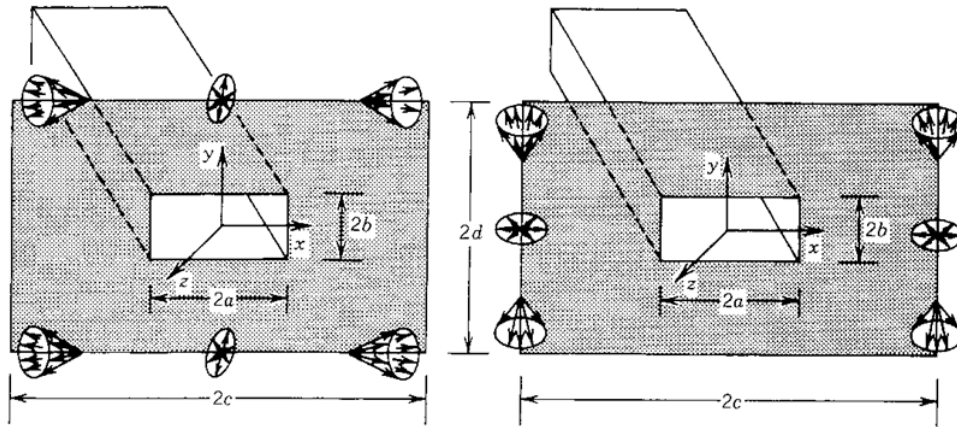


Figure 35: E- and H-plane Diffraction by a Rectangular Waveguide. *Figure Copied From [31 pg. 808]*

6.3.1 8.3 GHz Data

The data taken for (8.3 GHz) is in good agreement for the predicted and measured results, the main beam peak points to (19^0) for the predicted and (18.88^0) for the measured. The figures below are the far patterns, Figure 36 is the predicted pattern and Figure 37 is the measured pattern. Figure 38 is the predicted and measured combined patterns.

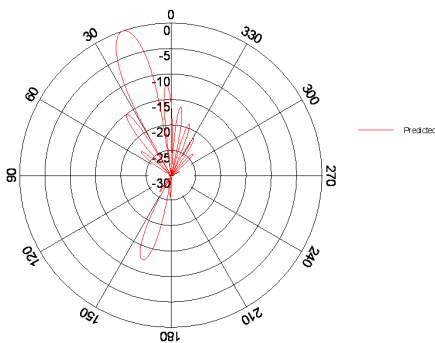


Figure 36

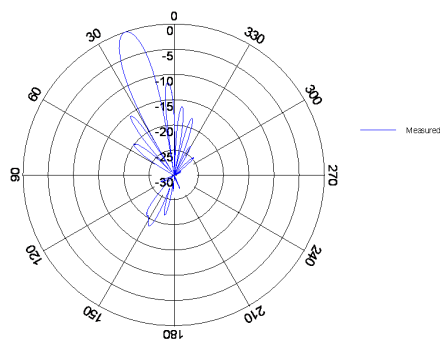


Figure 37

These are the (8.3 GHz) predicted data Figure 36 and measured data Figure 37 normalized gain plots, with a constant azimuth (270^0) and varying elevation.

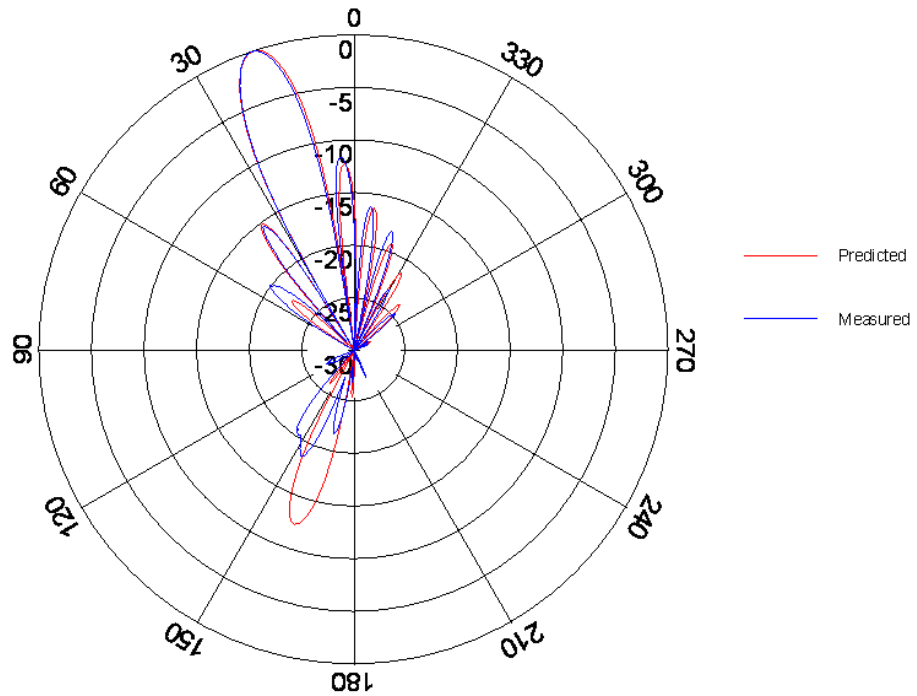


Figure 38: (8.3 GHz) Combined Normalized Gain Plot, With a Constant Azimuth (270°) and Varying Elevation

6.3.2 9.3 GHz Data

The data taken for (9.3 GHz) is in good agreement for the predicted and measured results, the main beam peak points to (7°) for the predicted and (8.25°) for the measured. The figures below are the far patterns, Figure 39 is the predicted pattern and Figure 40 is the measured pattern. Figure 41 is the predicted and measured combined patterns.

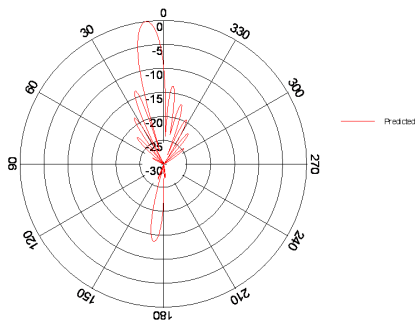


Figure 39

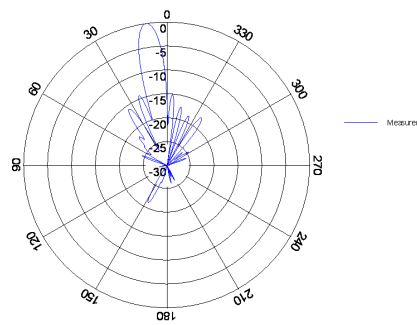


Figure 40

These are the (9.3 GHz) predicted data Figure 39 and measured data Figure 40 normalized gain plots, with a constant azimuth (270°) and varying elevation.

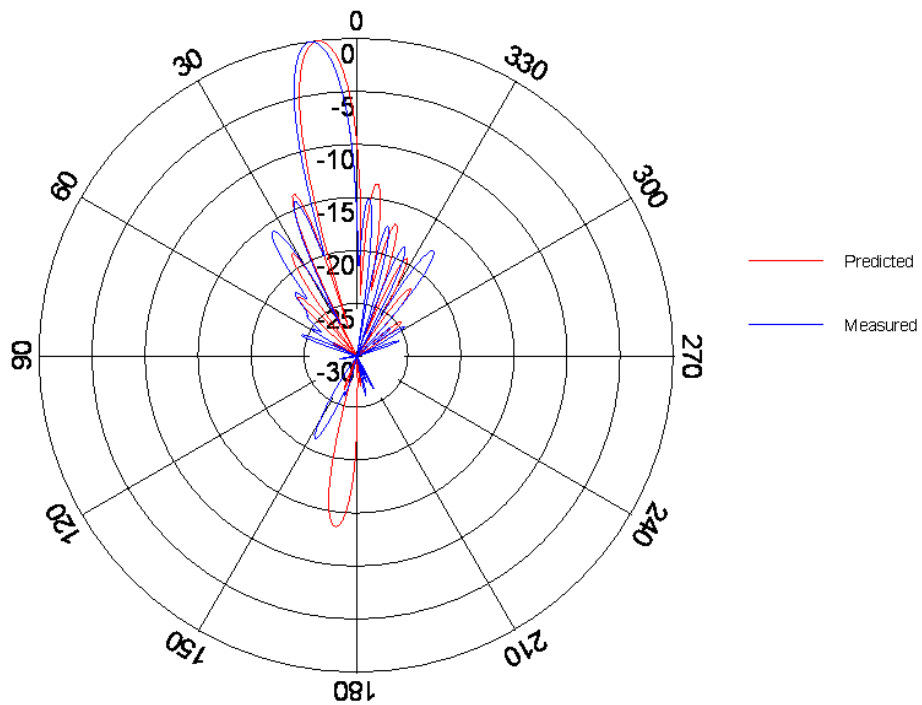


Figure 41: (9.3 GHz) Combined Normalized Gain Plot, With a Constant Azimuth (270°) and Varying Elevation

6.3.3 10.3 GHz Data

The data taken for (10.3 GHz) is in good agreement for the predicted and measured results, the main beam peak points to (359.0°) for the predicted and (360.0°) for the measured. The figures below are the far patterns, Figure 42 is the predicted pattern and Figure 43 is the measured pattern. Figure 44 is the predicted and measured combined patterns. Notice the backlobe pointing at (180°) for the predicted data and see that it is not there for the measured data. This is due to mounting the antenna in front of the phi rotator, Figure 29, and the backlobe diffracting around the rotator and splitting into two backlobes at $(\sim 155^{\circ})$ and $(\sim 205^{\circ})$.

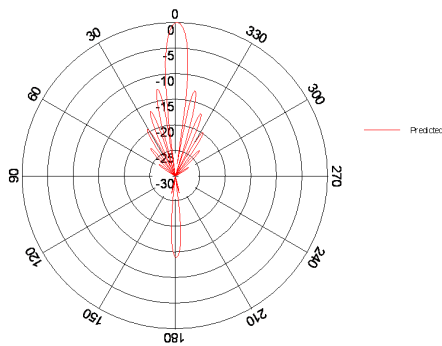


Figure 42

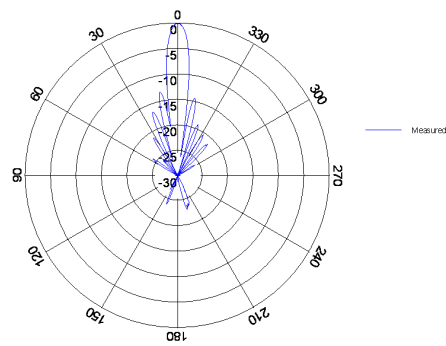


Figure 43

These are the (10.3 GHz) predicted data Figure 42 and measured data Figure 43 normalized gain plots, with a constant azimuth (270°) and varying elevation.

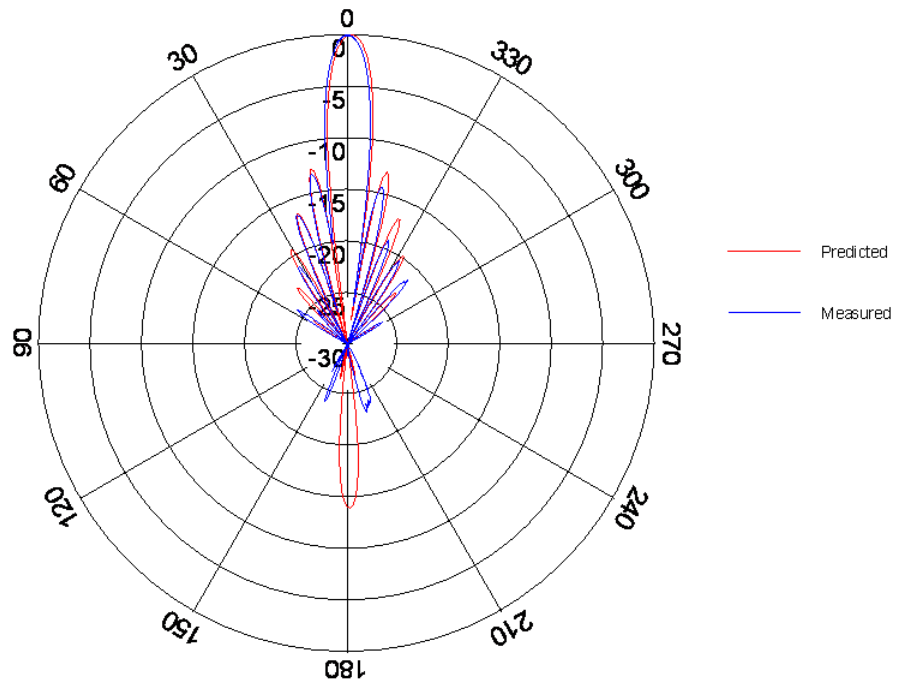


Figure 44: (10.3 GHz) Combined Normalized Gain Plot, With a Constant Azimuth (270°) and Varying Elevation

6.3.4 11.3 GHz Data

The data taken for (11.3 GHz) is in good agreement for the predicted and measured results, the main beam peak points to (353.0°) for the predicted and (354.0°) for the measured. The figures below are the far patterns, Figure 45 is the predicted pattern and Figure 46 is the measured pattern. Figure 47 is the predicted and measured combined patterns.

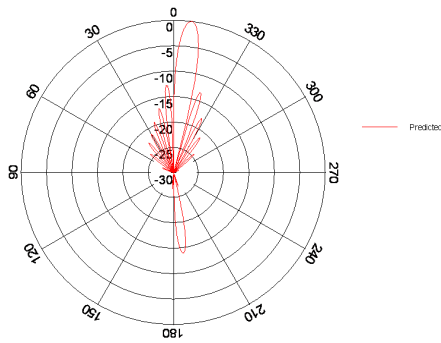


Figure 45

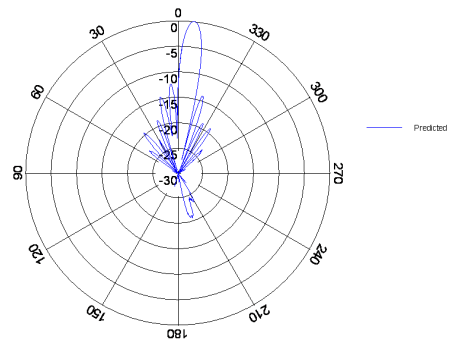


Figure 46

These are the (11.3 GHz) predicted data Figure 45 and measured data Figure 46 normalized gain plots, with a constant azimuth (270°) and varying elevation.

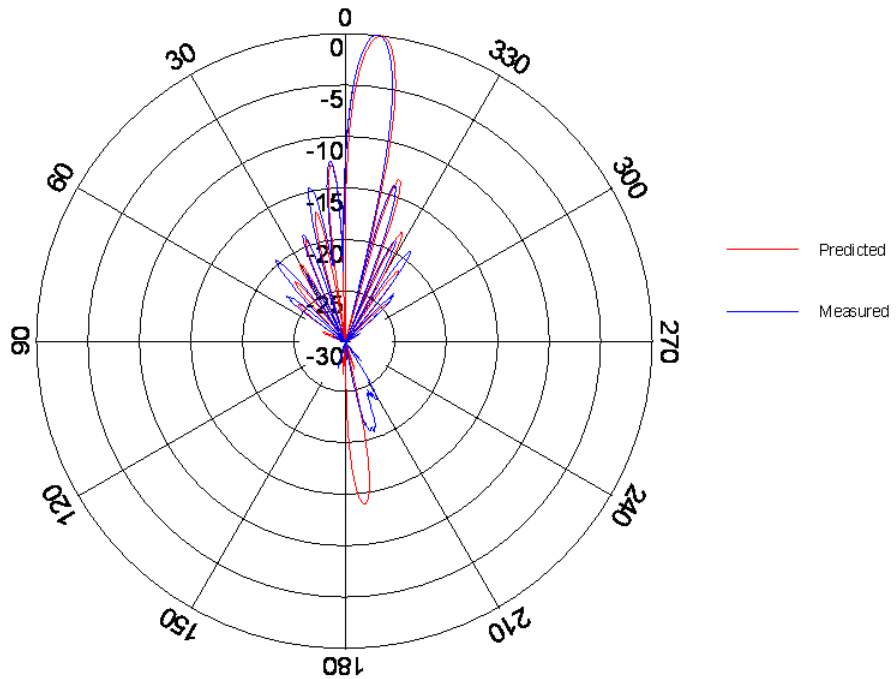


Figure 47: (11.3 GHz) Combined Normalized Gain Plot, With a Constant Azimuth (270°) and Varying Elevation

6.3.5 12.3 GHz Data

The data taken for (12.3 GHz) is in good agreement for the predicted and measured results, the main beam peak points to (348.0°) for the predicted and (348.37°) for the measured. The figures below are the far patterns, Figure 48 is the predicted pattern and Figure 49 is the measured pattern. Figure 50 is the predicted and measured combined patterns.

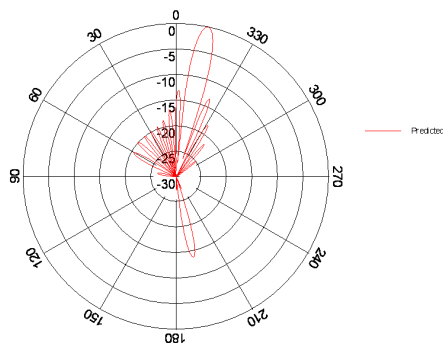


Figure 48

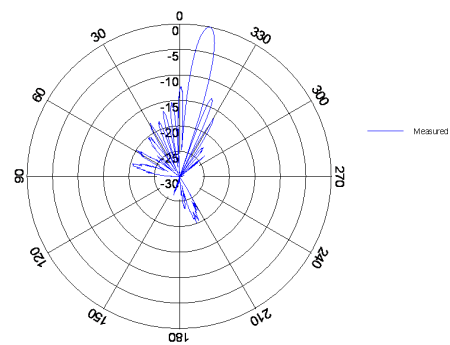


Figure 49

These are the (12.3 GHz) predicted data Figure 48 and measured data Figure 49 normalized gain plots, with a constant azimuth (270°) and varying elevation

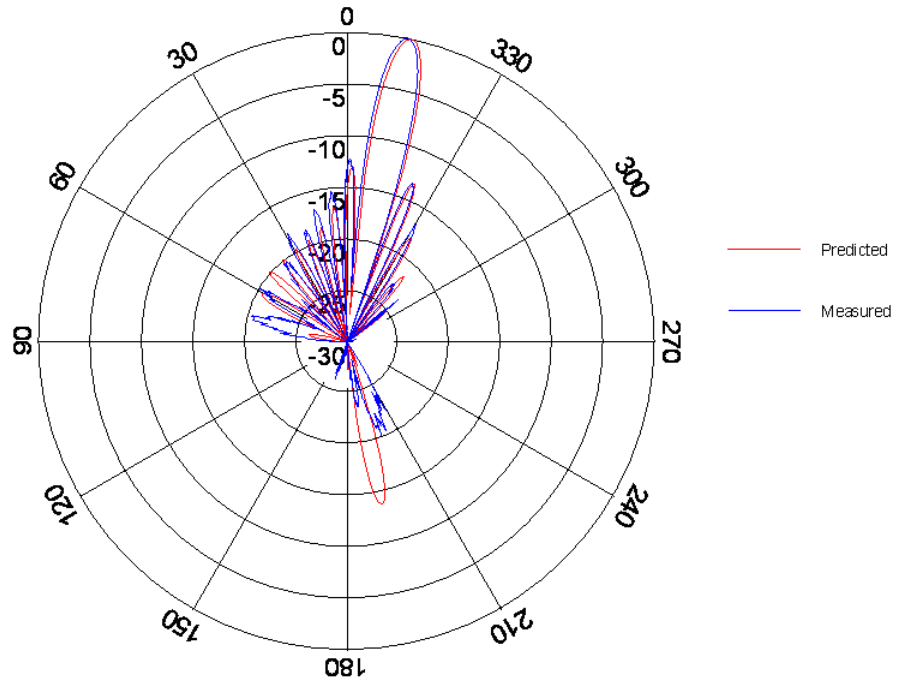


Figure 50: (12.3 GHz) Combined Normalized Gain Plot, With a Constant Azimuth (270°) and Varying Elevation

6.3.6 LC Parameter Extraction Prediction Results

The main beam angle (θ_{MB}) predictions are in Table 1. The polar plot in Figure 51 shows (90°) at broadside, endfire to the right of broadside, and backfire to the left of broadside. The LWA's fundamental frequency (f_0) is (10.3 GHz) and the table below shows it is not at broadside. None of the predictions in Table 1 below or on the polar plot in Figure 51 show the correct predicted main beam angle. If the predictions were correct, then the frequencies (8.3 GHz and 9.3 GHz) would be to the left of broadside, backfire, and the frequencies (11.3 GHz and 12.3 GHz) would be to the right of broadside, endfire. The suspected reason for the incorrect predictions is the lack of mutual coupling in the prediction equations. Another possible explanation for the LC parameter extraction

predictions being incorrect is the application of the Babinet-Booker Principle in determining the slot impedance.

Frequency	8.3 GHz	9.3 GHz	10.3 GHz	11.3 GHz	12.3 GHz
Angle (degree)	86.964	81.088	76.292	72.275	68.844

Table 1: LC Parameter Extraction Main Beam Predictions

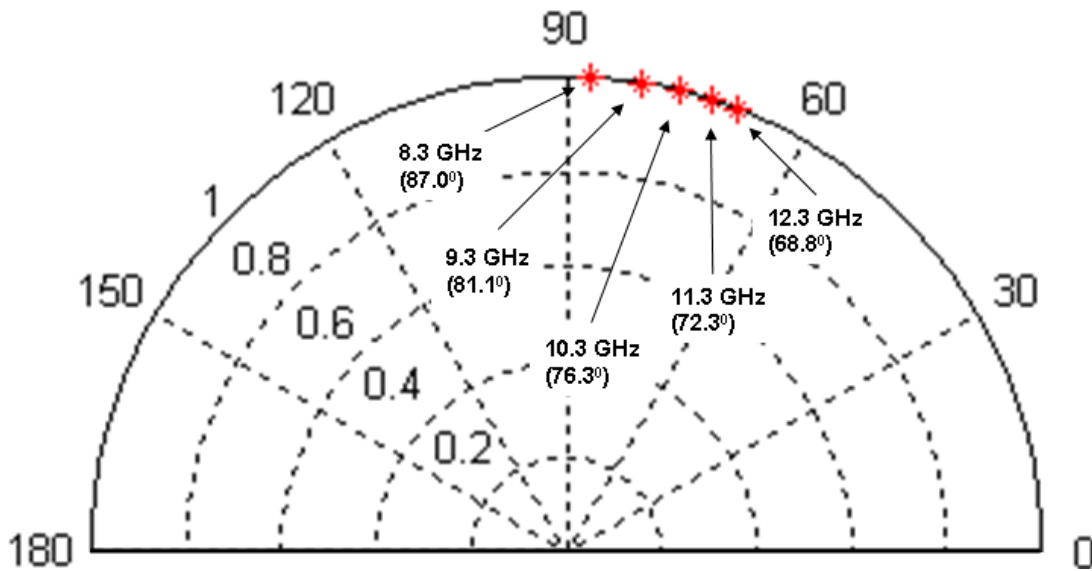


Figure 51: LC Parameter Predictions on a Polar Plot

7.0 Conclusion

In this research there are three different approaches in determining the main beam angle (θ_{MB}). The first approach used the metamaterial LC parameter extraction developed by C. Caloz and T. Itoh. The second approach was a full wave 3-D simulation using CARLOS and the third was a prototype that was measured. The LC parameter extraction did not work in this case due to the mutual coupling that takes place with tilted slot leaky

wave antenna, or possibly due to the Babinet-Booker Principal as mentioned previously. If the LC parameter extraction approach would have worked it would have let the designer design a portion of the radiating structure by using the parameters extracted from the single unit cell: C_L , L_L , C_R , and L_L . The full wave simulator approach and prototype antenna did have good agreement. The results show that tilted slot leaky wave antenna can radiate at broadside and move through both the right and left of broadside at the dominate mode (TE_{10}) by scanning the frequency. The radiation patterns show a relative narrow beam and the measured data shows the physical interaction between the antenna and the mounting pole, unlike the ideal conditions in the full wave simulator.

8.0 Future Work

There remains an opportunity for continued work on this problem. The mutual coupling needs to be accounted for in calculating the main beam pointing angle (θ_{MB}). This would give greater insight in the type of radiating element that may be used on a given antenna by showing how the elements interact with each other. This would also allow a wider range of radiating structures to use (42) in determining main beam radiation angles. Other future work is determining if the Babinet-Booker Principle was applied correctly.

Bibliography

1. Watson, W. H. "The Physical Principles of Waveguide Transmission and Antenna Systems," Oxford University Press, New York, 1947.
2. Oliner, A. A. "The Impedance Properties of Narrow Radiating Slots in the Broad Face of Rectangular Waveguide. Part I – Theory." IRE Transactions on Antennas and Propagation Jan., 1957.
3. Oliner, A. A. "The Impedance Properties of Narrow Radiating Slots in the Broad Face of Rectangular Waveguide. Part II– Comparison with Measurements." IRE Transactions on Antennas and Propagation Jan., 1957.
4. Ramsay, J. F., Popovich, B. V. "Series-Slotted Waveguide Array Antennas." Cutler-Hammer, Inc., Deer Park, NY, USA. IRE International Convention Record Vol. 11, pg. 30-55, Mar. 1963.
5. Elliott, R. S. Antenna Theory and Design. Englewood Cliffs, New Jersey: Prentice-Hall, Inc, 1981.
6. Veselago, V. "The electrodynamics of substances with simultaneously negative values of ϵ and μ ," Soviet Physics Uspekhi, vol. 10, no. 4, pp. 509–514, 1968.
7. Pendry, J.B. "Negative refraction makes a perfect lens," Phys. Rev. Lett., vol. 85, pp. 3966–3969, Oct. 2000.
8. Shelby, R.A., Smith, D.R. and Schultz, S. "Experimental verification of a negative index of refraction," Science, vol. 292, no. 5514, pp. 77–79, 2001.
9. Eleftheriades, G. V., Siddiqui, O. and Iyer, A.K. "Transmission line models for negative refractive index media and associated implementations without excess

- resonators,” *IEEE Microwave Wireless Compon. Lett.*, vol. 13, pp. 51–53, Feb. 2003.
10. Oliner, A. A., “A Periodic-Structure Negative-Refractive-Index Medium without Resonant Elements”. *IEEE-AP-S Digest*, San Antonio, TX p. 41. 2002.
 11. Caloz, C., and Itoh, T. Electromagnetic Metamaterials: Transmission Line Theory and Microwave Applications. Hoboken, New Jersey: John Wiley & Sons, Inc. 2006.
 12. Caloz, C., Sanada, A., and Itoh, T. “A Novel Right/Left-Handed Coupled-Line Directional Coupler with Arbitrary Coupling Level and Broad Bandwidth.” IEEE Transactions on Microwave Theory and Techniques Vol. 52, No. 3, March 2004.
 13. Caloz, C. and Itoh, T. “Transmission Line Approach of Left-Handed (LH) Materials and Microstrip Implementation of an Artificial LH Transmission Line.” IEEE Transactions on Antennas and Propagation Vol. 52, No. 5, May, 2004.
 14. Liu, L., Caloz, C., and Itoh, T. “Dominant Mode Leaky Wave Antenna with Backfire-to-Endfire Scanning Capability.” Electronic Letters Vol. 38, No. 23, Nov. 7th, 2002.
 15. Caloz, C. and Itoh, T. “Invited – Novel Microwave Devices and Structures on the Transmission Line Approach of Meta-Materials.” IEEE MTT-S Digest, 2003.
 16. Lai, A., Caloz, C., and Itoh, T. “Composite Right/Left-Handed Transmission Line Metamaterials.” IEEE Microwave Magazine Sept. 2004.
 17. Caloz, C., Itoh, T., and Rennings, A. “CRLH Metamaterial Leaky-Wave and Resonant Antennas.” IEEE Transactions on Antennas and Propagation Vol. 50, No. 5, October, 2008.

18. Johnson, R. C. Antenna Engineering Handbook 3rd Edition. New York: McGraw-Hill, 1993.
19. Harrington, R. F. Time-Harmonic Electromagnetic Fields. New York: McGraw-Hill, 1961.
20. Jordan, E. C. Electromagnetic Waves and Radiating Systems. Englewood Cliffs, New Jersey: Prentice-Hall, Inc. 1950.
21. Pozar, D. M. Microwave Engineering 2nd Ed. New York: Wiley, 1998.
22. Ulaby, F. T. Fundamentals of Applied Electromagnetics 2001 Media Ed. Upper Saddle River, New Jersey: Prentice-Hall, Inc. 2001.
23. Kraus, J. D. Antennas 2nd Edition. New York: McGraw Hill. 1988.
24. Milligan, T. Modern Antenna Design. . New York: McGraw-Hill Book Company, 1985.
25. Richmond, J. H. “Mutual Impedance between Coplanar-Skew Dipoles.” IEEE Transactions on Antennas and Propagation May 1970.
26. Richmond, J. H. and Geary, N. H. “Mutual Impedance between Coplanar-Skew Dipoles.” Department of the Army Ballistic Research Laboratory Aberdeen Proving Ground Maryland 21005, Technical Report 2708-2. Contract No. DAAD05-69-C-0031. Aug. 6th, 1969.
27. Orfanidis, S. J. Electromagnetic Waves and Antennas. 2008.
www.ece.rutgers.edu/~orfanidi/ewa/
28. Collin, R. E. and Zucker, F. J. Antenna Theory Part 1. New York: McGraw-Hill Book Company, 1969.

29. Balanis, C. A. Antenna Theory and Analysis and Design 3rd Ed. Hoboken, New Jersey: John Wiley & Sons, Inc. 2005.
30. Putnam, J. M, Medgyesi-Mitschang, L. N, and Gedera, M. B. "CARLOS 3-D Three Dimensional Method of Moments Code: Vol. 1: Theory and Code Manual" St. Louis: New Aircraft and Missile Products McDonnell Douglas Aerospace-East, 1992.
31. Balanis, C. A. Advanced Engineering Electromagnetics. Hoboken, New Jersey: John Wiley & Sons, Inc. 1989.
32. Collin, R. E. Field Theory of Guide Waves. New York: McGraw-Hill, 1960.
33. Collin, R. E. Foundations for Microwave Engineering. New York: McGraw-Hill Book Company, 1966.
34. Collin, R. E. and Zucker, Francis J. Antenna Theory Part 2. New York: McGraw-Hill Book Company, 1969.
35. Sadiku, M. N.O. Elements of Electromagnetics 3rd Ed. New York: Oxford U. Press, 2001.
36. Ramo, S., Whinnery, J. R and Van Duzer, T. Fields and Waves in Communications Electronics 3rd Ed. New York: John Wiley & Sons, Inc, 1994.
37. Engheta, N., and Ziolkowski, R. C. Metamaterials:Physics and Engineering Exploration. Piscataway, New Jersey: IEEE Press, 2006.
38. Elliott, R. S. An Introduction to Guided Waves and Microwave Circuits. Englewood Cliffs, New Jersey: Prentice Hall, 1993.
39. LePage, W. R. and Seely, S. General Network Theory. New York: McGraw-Hill Book Company, 1952.

40. Irwin, J. D. Basic Engineering Circuit Analysis. New York: John Wiley & Sons, Inc. 2002.
41. Ludwig, R., and Bretchko, P. RF Circuit Design: Theory and Applications. Upper Saddle River, New Jersey: Prentice-Hall, Inc. 2000.
42. Walter, C. H. Traveling Wave Antennas. Los Altos, California USA: Peninsula Publishing, 1990.
43. Stutzman, W. L. and Thiele, G. A. Antenna Theory and Design. New York: John Wiley & Sons, Inc. 1981.
44. Montgomery, C. G., and Dicke, R. H., and Purcell, E. M. Principles of Microwave Circuits. New York: McGraw-Hill Book Company Inc. 1948.
45. Ragan, G. L. Microwave Transmission Circuits. New York: McGraw-Hill Book Company Inc. 1948.
46. Marcuvitz, N. Waveguide Handbook. New York: McGraw-Hill Book Company Inc, 1951.
47. Silver, S. Microwave Antenna Theory and Design. New York: McGraw-Hill Book Company Inc, 1949.
48. King, H. E. "Mutual Impedance of Unequal Length Antennas in Echelon." IRE Transactions on Antennas and Propagation Jul. 1957.
49. Baker, H. C. and LaGrone, A. H. "Digital Computation of the Mutual Impedance between Thin Dipoles." IRE Transactions on Antennas and Propagation Jan., 1962.
50. Richmond, J. H. "Coupled Linear Antennas with Skew Orientation." IEEE Transactions on Antennas and Propagation, Sept. 1970.

51. Orefice, M. and Elliot, R. S. "Design of Waveguide-Fed Series Slot Arrays." IEE Proc., Vol. 129, Pt. H, No. 4, Aug. 1982.

Vita

Garrett Gilchrist

Date of Birth	September 23, 1976
Place of Birth	Wichita, Kansas
Degrees	B.S. Electrical Engineering, December 2004
Employment	The Boeing Company, January 2005, Computational Electromagnetics

December, 2010